Forest fire and its relationship to large-scale atmospheric circulation

Master thesis

Faculty of Science, University of Bern

handed in by

Michael Herrmann

2022

Supervisors

Prof. Dr. Stefan Brönnimann

Prof. Dr. Olivia Romppainen-Martius

Advisor

Dr. Daniel Steinfeld

Abstract

Heatwaves and droughts are exacerbated by climate change, increasing the potential of unprecedented fire prone weather conditions. It is therefore of great interest to better understand the occurrence of wildfires and the main drivers. Since the large-scale atmospheric circulation modulates the day-to-day surface weather and contributes to extremes like heatwaves and droughts, it could be a potential dynamical driver for increased fire danger. In this study, we investigate the influence of persistent large-scale atmospheric circulation patterns, such as atmospheric blocking, on the spatiotemporal variability of fire weather danger and active fires across Europe. We apply a co-location analysis method to quantify the relevance of atmospheric blocking for increased fire danger and occurrence. Atmospheric blocks are identified and tracked as daily Z500 anomalies based on ECMWF ERA5 reanalysis data. To describe daily fire weather danger, we use the Fire Weather Index (FWI) and the Fine Fuel Moisture Code (FFMC) based on the Canadian Fire Weather Index System provided by ECMWF ERA5 reanalysis, and satellite-observed active fires are obtained from the AVHRR sensor. Our results show that over large parts of Northern and Western Europe more than 80% of all extreme fire danger events occur simultaneously with atmospheric blocking at the same location. On the other hand, extreme fire danger events in Southern Europe are not associated with atmospheric blocks, but often occur under a subtropical ridge. Furthermore, we assess the capability of the FWI and atmospheric blocking as active fire indicators. 38%-52% of all observed active fires between 1991 and 2019 occur during fire prone weather conditions with FWI values above the 90th percentile (>P90), but the link to atmospheric blocking is not strong. The performance of the FWI in detecting active fires varies by region and season, with the best results in Eastern Mediterranean and winter for >P90. The strong relationship between atmospheric blocking and fire weather danger is important for both weather forecasting and climate change projections and indicates that such large-scale circulation patterns have the potential to improve the prediction of fire danger.

Table of Contents

List of Figures

List of Tables

List of Abbreviations

AF	Active Fire
AVHRR	Advanced Very High Resolution Radiometer
BUI	Build Up Index
DC	Drought Code
DJF	December – February (winter)
DMC	Duff Moisture Code
ECMWF	European Centre for Medium Range Weather Forecasts
EFDE	Extreme Fire Danger Event
FDE	Fire Danger Event
FFMC	Fine Fuel Moisture Code
FWI	Fire Weather Index
FWIS	(Canadian) Fire Weather Index System
ISI	Initial Spread Index
JJA	June – August (summer)
MAM	March – May (spring)
POD	Probability Of Detection
Pxx	xx^{th} Percentile
SON	September – November (autumn)
Z500	500-hPa geopotential height

1 Introduction

1.1 Motivation

Wildfires are an integral part of the natural Earth system dynamics, but they are becoming more devastating with anthropogenic climate change (Vitolo et al. 2020). Recent years, including 2022, have seen record-breaking fire seasons across the world. The impacts of wildfires are diverse, ranging from loss of property and resources to the deterioration of the air quality and entailing health issues. Another example of the ramifications is the drastic increase in global insured losses due to wildfires over the last four decades (Figure 1.1). The total losses increased from USD 10 billion in the period of 2000-2009 to USD 45 billion in the subsequent decade (SwissRe 2021). Not only did the total insured losses from wildfires increase, but its fraction of total natural catastrophe losses also increased significantly to almost 14% in 2020. Climate change and land-use change exacerbate the threat and lead to a global increase of extreme fires even in areas previously unaffected (UNEP 2022). Therefore, with rising global temperatures it is crucial to better understand the variability of fire danger and to reduce vulnerability to wildfires.

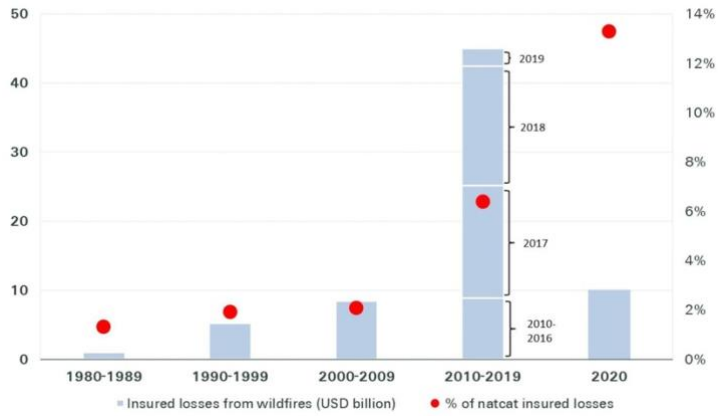

Figure 1.1: Global insured losses from wildfires since 1980 by decade (USD billion), at 2020 prices (Source: SwissRe).

The meteorological conditions that would cause flames to spread if ignited are named fire weather (Vitolo et al. 2020). Fire weather is based on atmospheric variables such as temperature, precipitation, relative humidity, and wind speed. Previous studies have shown that fires spread rapidly when the fuels are dry, and the weather conditions are hot, dry, and windy (Flannigan and Wotton 2001). In recent decades, the fire weather season has lengthened and become more severe in many parts of the globe (Jolly et al. 2015, Vitolo et al. 2020). Wildfires affect various sectors such as ecosystems, forestry, and human health (IPCC 2021). According to the latest IPCC (2021) report AR6, fire weather is projected to increase with high confidence in e.g., the Mediterranean, North America, and Australia. For this reason, it is of key interest to better understand the occurrence and the main drivers of wildfires.

Generally, four factors determine wildfire activity: fuel availability, weather and climate, ignition agents, and anthropogenic factors (Jain and Flannigan 2021). In fact, as Di Giuseppe et al. (2016, p. 2469) state: "where fuel is available, weather is the most important factor in shaping fire regimes". Thus, for fire management purposes, fire weather indices have been developed to describe the near-surface atmospheric conditions conducive to fire occurrence and spread (Van Wagner 1987). Van Wagner (1987) developed the Canadian Fire Weather Index System (FWIS), which is commonly used to provide daily information on fire weather danger. The FWIS consists of six components: three fuel moisture codes and three fire behavior indices. They represent a combined metric that expresses the probability of fire ignition, the speed and likelihood of spread, and the fuel availability (Di Giuseppe et al. 2016).

Fire weather indices only indicate a potential danger and not whether there is actually a fire, as it is dependent on an ignition source. The information on fire causes in Europe is very uncertain with half of the fire records lacking a known cause (de Rigo et al. 2017). However, where information is available, in more than 95% of the cases fires in Europe are ignited due to human activity, either because of arson, human negligence or accidents (Figure 1.2) (de Rigo et al. 2017, Ganteaume et al. 2013). Since humans are the primary source of fire ignition, it is very difficult to estimate the occurrence of fires accurately. Thus, in this thesis, we evaluate the capability of the fire weather indices to effectively flag regions as high fire weather danger when actual fire events occurred (Di Giuseppe et al. 2016).

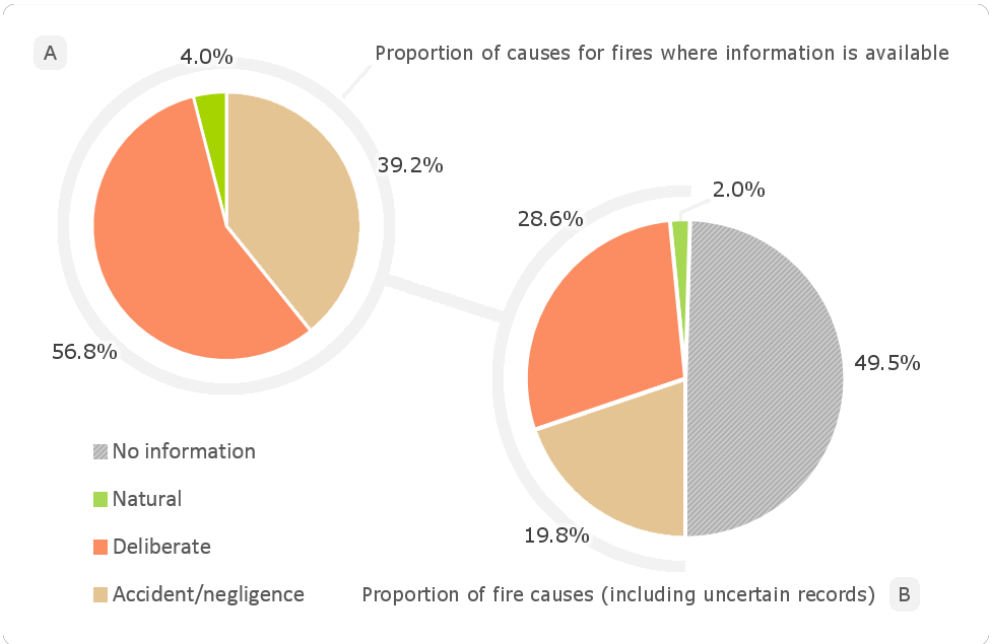

Figure 1.2: Causes of wildfires as reported by 19 European countries (Bulgaria, Croatia, Cyprus, Estonia, Finland, France, Germany, Greece, Hungary, Italy, Latvia, Lithuania, Poland, Portugal, Romania, Slovenia, Spain, Sweden, Switzerland). (A) Wildfires where information on their causes is available and (B) Wildfires with those lacking a known cause. (Source: de Rigo et al. 2017)

Previous studies have investigated the influence of the large-scale atmospheric circulation on extreme weather events such as temperature extremes or heavy precipitation events (Lenggenhager and Martius 2019, Mastrantonas et al. 2021, Pfahl and Wernli 2012a). The impact of weather patterns increases when they persist for several days or weeks. In the midlatitudes, Rossby (or planetary) waves manifest as a meandering jet stream associated with ridges and troughs across the earth's hemisphere. Persistent ridges or anticyclones, commonly referred to as atmospheric blocking, describe an anticyclonic quasi-stationary flow pattern, which is a fundamental characteristic of mid-latitude weather (Matsueda and Endo 2017, Woollings et al. 2018). These blocking anticyclones have been found mostly responsible for temperature extremes that lead to heatwaves or drought events at the surface (Horton et al., 2016, Pfahl and Wernli 2012a, Teng and Branstator 2017). Subsidence and clear-sky radiative forcing associated with the central part of the block can lead to surface hot temperature extremes (Pfahl and Wernli 2012a). In addition, the coupling of the atmosphere with soil moisture by enhancing surface evaporation can cause a depletion of soil moisture. Exactly these hot and dry surface conditions are the prerequisites for the occurrence of increased fire weather danger.

Since the upper-level circulation modulates the surface weather variability, it could be a potential driver of fire weather danger (Flannigan and Wotton 2001, Jain and Flannigan 2021). Several studies have shown a robust correlation between the area burned and positive 500-hPa geopotential height anomalies, namely anticyclonic features such as ridges and blocks in North America (Hostetler et al., 2018, Macias Fauria and Johnson 2006). Blocking anticyclones are commonly associated with an extreme fire weather danger in North America (Jain and Flannigan 2021). Additionally, several studies have examined the connection of weather patterns and wildfires for specific regions such as Portugal or Spain, but not on a larger continental scale (Hoinka et al. 2009, Rasilla et al. 2010, Wastl et al. 2013).

Large-scale circulation patterns like 500-hPa geopotential height (Z500) are better forecasted than surface fields in global sub-seasonal to seasonal (S2S) models (Yano et al. 2018). Therefore, a better understanding of the relationship between Z500 and fire weather danger could improve the confidence and help to identify regions that could experience above average fire weather danger a few weeks in advance. Furthermore, fire management agencies operate with a narrow margin between success and failure (Jain and Flannigan 2021). For this reason, it is important and beneficial for them to better understand the spatiotemporal characteristics of fire weather danger for future management strategies.

As introduced, several studies investigated the relationship of the large-scale atmospheric circulation and surface extremes of temperature or precipitation. However, a pan-European investigation of the relationship between weather patterns and wildfires is still lacking. This is the reason why in this thesis, we investigate the spatiotemporal variability of fire weather danger and actual fire occurrence in Europe

as well as the role of large-scale weather patterns, such as blocking, as a potential driver for extreme fire weather danger.

1.2 Aims of the thesis

The main goal of this master thesis is to better understand the spatial and temporal characteristics of fire weather danger in Europe and the relationship to large-scale atmospheric circulation patterns. Understanding the mechanisms behind the occurrence of extreme fire danger is important to estimate their frequency and intensity in a changing climate. To achieve these goals, the subsequent research questions are addressed:

- Which weather patterns were important during the extreme fire season in Europe in 2018?
- What is the influence of persistent large-scale circulation patterns, such as atmospheric blocking, on the spatiotemporal variability of fire weather danger and satellite-observed active fire occurrence?
- How accurate do fire weather indices detect satellite-observed active fires?

The structure of the thesis is as follows. In Chapter 2.1, we describe the data that we use and in Chapter 2.2 the methods that we apply. In Chapter 3, we present the results, which we discuss in Chapter 4. In Chapter 5, we sum up our analysis and provide an outlook on possible future studies.

2 Data and Methods

2.1 Data

In this master thesis, we use ERA5 reanalysis data from the European Centre for Medium Range Weather Forecasts (ECMWF). The ERA5 reanalysis dataset is based on model forecasts from the Integrated Forecasting System (IFS) Cy41r2 and the 4D-Var data assimilation (Hersbach et al. 2020). It covers the time period from 1979 to today and provides hourly estimates of many atmospheric, land and oceanic climate variables. Reanalysis datasets provide a spatially and temporally homogeneous alternative to point-based observations and are the consistent gridded history of the weather (Figure 2.1). With a horizontal resolution of 31 km and 137 levels from the surface up to 80 km, ERA5 captures much finer details of atmospheric phenomena than its predecessor ERA-Interim (Hersbach et al. 2020). Above all, the new fire danger reanalysis dataset based on ERA5 provides some improvement compared to ERA-Interim in the estimation of precipitation and evaporation and has a higher spatial resolution. For these reasons, fire reanalysis products can be used as a proxy for fire weather observations and can advance fire science (Vitolo et al. 2020).

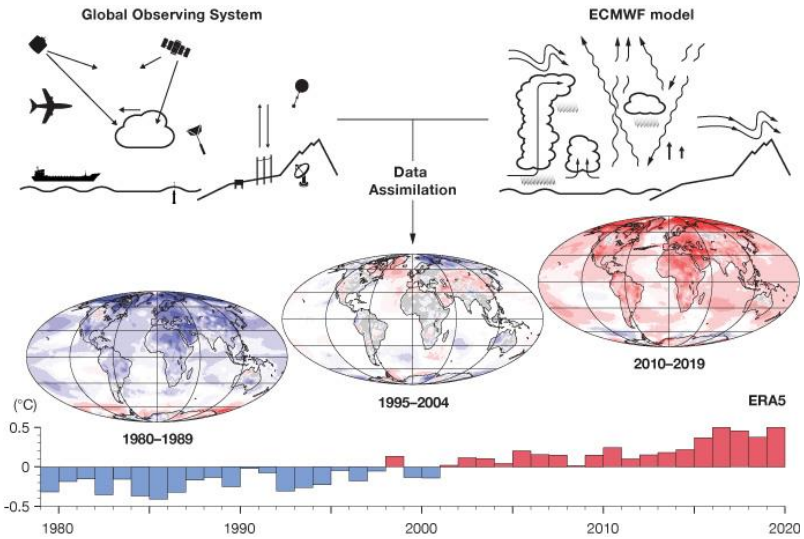

Figure 2.1: Schematic representation of the reanalysis process (Source: ECMWF 2020)

We use different fields from ERA5 with various temporal and spatial resolutions. To calculate the fire weather indices defined by the Canadian Forest Service, surface temperature, humidity, precipitation, and wind fields are used on a 0.25° grid and with daily resolution (Hersbach et al. 2020, Van Wagner 1987). Additionally, we use Z500 to describe large-scale blocking patterns. All the fields are available for the entire Northern Hemisphere from 1979 to 2020. In addition to ERA5 reanalysis data, we use active fire masks derived from satellite data retrieved with the Advanced Very High Resolution Radiometer (AVHRR) (Weber and Wunderle 2019).

2.1.1 ERA5 Reanalysis Data

In the following, the specific ERA5 and satellite data that is used for this master thesis will be described.

2.1.1.1 Fire Weather Indices

The fire weather danger data from the Canadian Forest Service Fire Weather Index Rating System (FWIS) is derived from modelled data using weather forecast from historical simulation provided by ERA5 reanalysis data (Di Giuseppe 2021). The FWIS describes the influence of four atmospheric variables (temperature, humidity, precipitation, and wind speed) on the fuel moisture content and, consequentially, also on the fire behaviour and occurrence (Di Giuseppe et al. 2016). The system depends solely on these four weather variables taken at 12:00 local time when the condition for wildfire is most favourable (Di Giuseppe et al. 2016, Van Wagner 1987). The FWIS is calibrated to describe the fire behaviour in jack pine stands (*Pinus banksiana*), typical for Canadian forests for which the index system was originally developed (Van Wagner 1987). However, despite this inherent limitation, the FWIS is being successfully used in other countries where the vegetation differs from the one in Canada (Di Giuseppe et al. 2016). For example, southern Portugal shows a good correlation of the FWI and fire activity (Viegas et al. 1999).

In the FWIS, the fuel moisture content is evaluated, and then relative fire behavior codes are calculated using the past and present effect of weather on forest floor fuels (Van Wagner 1987). The FWIS is comprised of six components divided into two groups: the first one contains three fuel moisture codes, and the second one three fire behaviour indices (Figure 2.2). The fuel moisture codes consist of the Fine Fuel Moisture Code (FFMC), Duff Moisture Code (DMC), and the Drought Code (DC). The fire behaviour index group includes the Initial Spread Index (ISI), the Build Up Index (BUI), and the final Fire Weather Index (FWI), which combines all previous subindices (Van Wagner 1987). The FWI, which is the most commonly used index, rates the potential fire intensity and provides the general public information about fire danger conditions (Di Giuseppe 2021). The FFMC, on the other hand, reflects the moisture content of the litter layer (1-2 cm deep) and is characterized by a rapid reaction to dryness or precipitation. For this reason, the FFMC describes the day-to-day variability of fire weather danger in a better way than the FWI. The DMC is an indicator of moisture content in moderate depth (5-10 cm deep), of the loosely compacted organic layers (Van Wagner 1987). The drying rate is slower compared to the FFMC with a time lag of 12 days. The DC indicates the moisture content of deep and compact organic layers (Van Wagner 1987). It represents a lower fuel layer at 10-20 cm depth where the soil dries the slowest with a lag of 52 days. The last two indices, the ISI and the BUI, describe the expected rate of fire spread and the total amount of fuel that is available for combustion, respectively.

In this thesis, we use the FWI and the FFMC in order to investigate one index of each subgroup and to have one general fire danger index (FWI) and one that describes better the day-to-day variability (FFMC). For the case study of summer 2018, we look at the temporal evolution of all subindices.

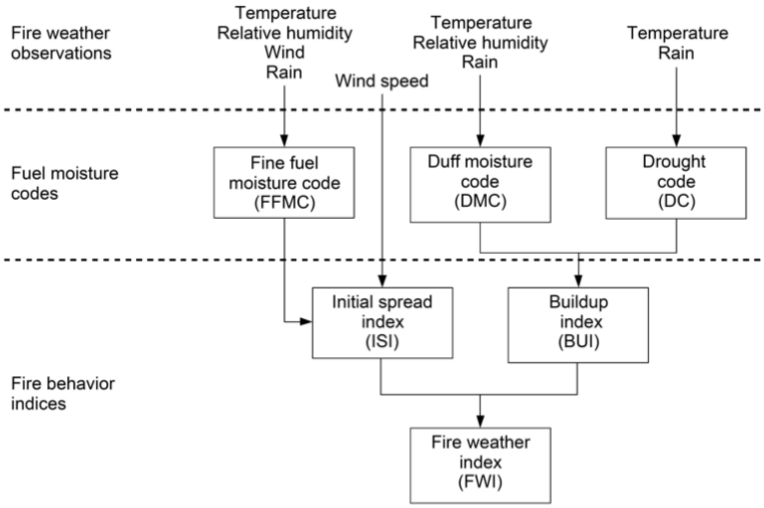

Figure 2.2: Structure of the Canadian Forest Fire Weather Index System (FWIS) describing the six components and the respective input variables (Source: Van Wagner, 1987)

2.1.1.2 Atmospheric Blocking

Blocking that persists for weeks can induce extreme meteorological conditions at the surface such as temperature anomalies (Matsueda and Endo 2017). This is the reason why blocks are an integral part of this thesis for investigating the spatiotemporal variability of fire weather danger and the role of large-scale circulation patterns. We modified the Schwierz et al. (2004) algorithm to calculate blocks based on Z500 anomalies with respect to the climatological 30 day-running mean of the analyzed period (1979-2020). Technically, we use a 50% spatial overlap between the blocked areas of successive days for at least 5 days. Blocked areas are identified as positive Z500 anomalies above a daily varying intensity threshold defined as the 90^{th} percentile of the Z500 long-term daily anomaly distribution over 30°N-90°N and smoothed further with a Fast Fourier Smoothing. A variable threshold captures more blocks in summer, especially at lower latitudes, which is an improvement from the original algorithm. Figure 2.3 shows the seasonal blocking frequencies derived from ERA5. We describe the seasonal blocking frequencies of Europe at the end of Chapter 3.2.

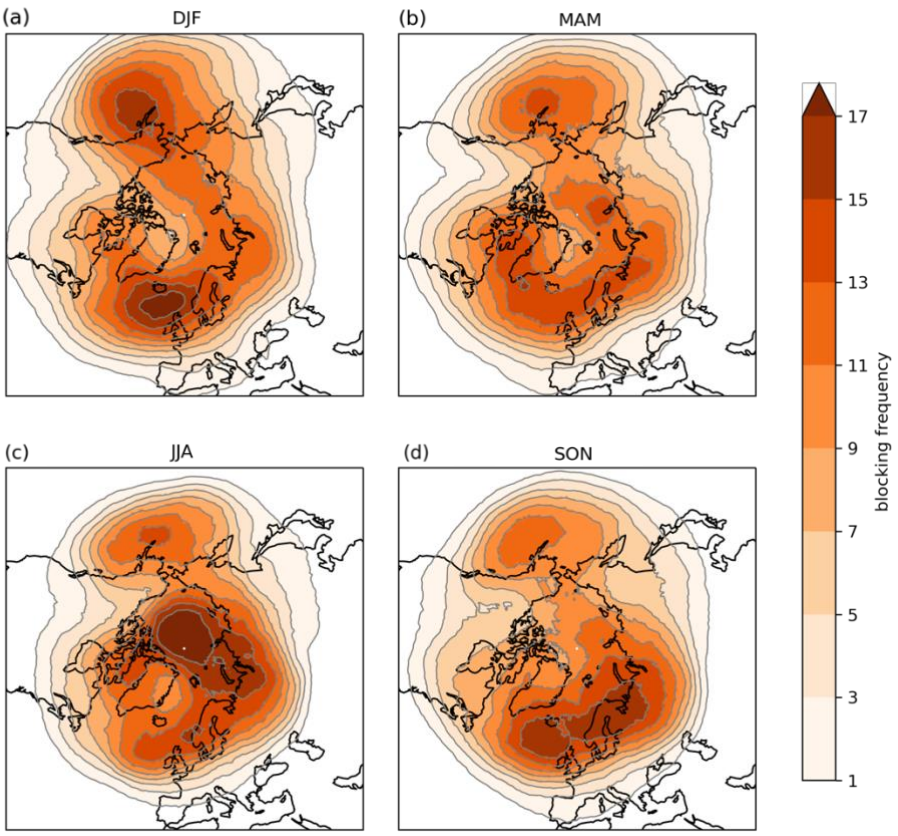

Figure 2.3: Seasonal blocking frequencies in % for four seasons over the Northern Hemisphere based on Z500 anomalies (adapted from Schwierz et al. 2004).

2.1.2 AVHRR Satellite Data

Fire weather indices only describe a potential danger, which means that a high meteorological fire danger does not automatically imply the occurrence of a forest fire (Wastl et al. 2013). Therefore, in order to investigate the actual fire occurrence, we integrate satellite data of observed fires into the analysis. The dataset of interest is imagery of the heritage Advanced Very High Resolution Radiometer (AVHRR). It is a long-term active fire dataset with a daily resolution and covering the period of 1985-2020 and a spatial resolution of 1.1 km^2 (at nadir) (Weber and Wunderle 2019). In this thesis, we will investigate the satellite data for the WMO climatological period from 1991 to 2019. The year 2020 is missing as it has not been processed yet.

The AVHRR sensor is onboard a series of National Oceanic and Atmospheric Administration (NOAA) and Meteorological Operational (MetOp) satellites (Weber and Wunderle 2019). The sensor is utilized for operational meteorology, which includes measuring cloud properties, land analysis by supplying data to calculate vegetation indices, and ocean analysis by measuring sea surface temperature (Kalluri

et al. 2021). Thus, the sensor was initially not constructed for fire detection per se, but its radiometric measurements can be used to derive active fires masks.

The active fire product consists of binary fire masks including confidence estimates for each fire pixel. A prerequisite for the detection of active fires is the activation of the mid-infrared (MIR) channel of the AVHRR sensor. To detect an active fire, the spectral response of a subpixel fire in the MIR is compared to its background MIR and thermal infrared measurements (Weber and Wunderle 2019). In doing so, the sensor identifies the temperature difference in order to separate active fires from their cooler, fire-free background. This is achieved by iteratively thresholding using contextual algorithms after the initial identification of a potential fire pixel (Giglio et al. 1999, Weber and Wunderle 2019). The algorithm applies a fuzzy pixel approach using a matrix of 3 x 3 neighboring pixels around the potential fire pixel in order to verify the fire signal. The minimum detectable fire size by the AVHRR sensor ranges from 100m^2 for a flaming fire (>900K) to 1000m^2 for a smoldering fire (600K) and the maximum limit ranges from 10 000m^2 to 50 000m^2 for flaming and smoldering fires respectively (Giglio et al. 1999).

2.1.3 Definition of Study Regions

For this thesis we define four study regions: Northern Europe, Central Europe, Western Mediterranean, and Eastern Mediterranean. We use the Northern and Central Europe regions predefined by the SREX report (Iturbide et al. 2020). For Southern Europe, we use the two Mediterranean regions as used in the study of Zschenderlein et al. (2019). As can be seen in Figure 2.4, Western Mediterranean covers the Iberian Peninsula and Eastern Mediterranean covers mainly Italy and Greece. The Central European region spans zonally and includes Western Europe and parts of Eastern Europe while Northern Europe includes Great Britain and Scandinavia.

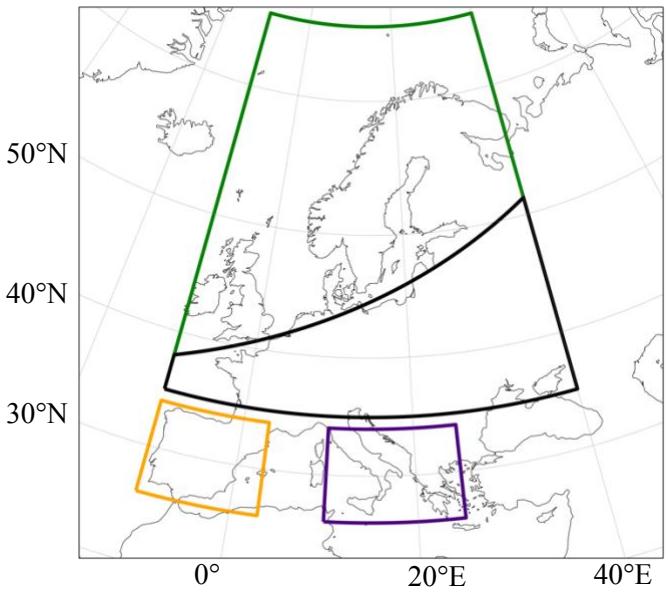

Figure 2.4: Study regions in Europe: Northern Europe (green box, SREX predefined region), Central Europe (black box, SREX predefined region), Western Mediterranean (orange box, 36°N–44°N, 10°W–3°E) and Eastern Mediterranean (indigo box, 36°N–44°N, 10°E–25°E). Northern Europe and Central Europe share one border of their box (the upper black line). Only land grid points in these boxes are selected.

2.1.4 Data Preparation

We use ERA5 reanalysis data to calculate atmospheric blocking and fire weather indices. The active fire masks are based on the AVHRR sensor. The ERA5 dataset covers the period of 1979-2020 and AVHRR dataset the WMO reference period 1991-2019. The spatial and temporal resolution in our analysis is 1° x 1° and daily for all fields. We look at three different seasons: spring (March – May, MAM), summer (June – August, JJA) and autumn (September – November, SON). All fields (blocking, FWI, active fire) are converted to binary masks with 1 = occurrence and 0 = no occurrence. In the following subsections, we describe the details of the initial data manipulation.

2.1.4.1 Fire Weather Indices

Since we look at the fire weather danger at every location, we look at the fire danger of all sorts of wildfires and not only forest fires. We define fire weather danger extremes based on the 95th, 97th and 99th percentiles (P95, P97 and P99) of the daily distribution of the two fire weather indices FWI and FFMC for the ERA5 period 1979-2020. In this thesis, if not stated otherwise, the days exceeding the P99 of the daily distribution for each grid cell are referred to as extreme fire danger events (EFDE).

2.1.4.2 Atmospheric Blocking

We calculate the blocking index (according to Chapter 2.1.1.2) and select the blocking data for the seasons MAM, JJA, and SON. We convert the data to binary fields with the information whether there was a block on each day and at the same location or not. We also carry out a lagged analysis, to account for the effect of atmospheric blocking during the preceding week. Technically, we count on how many days of the previous week a block was present at the respective grid cell. If there is a block on at least 4 out of 7 days, we assume it to be significant for the present-day fire weather danger and count it as a lagged match (1, otherwise 0).

2.1.4.3 AVHRR Active Fire

The resolution of the original data is approximately 1 x 1 km with several swaths per day depending on how many satellites passed over Europe that day. Since forested land cover obtained the best validation results, we only take forest areas into consideration. Thus, compared to the fire weather indices where we include all type of wildfires, here we only look at forest fires. Copernicus Land Cover Maps from the years 1990, 2000, 2006, 2012 and 2018 were used to select the desired forest grid points. More specifically, the following three forest types are used: broad-leaved forest, coniferous forest, and mixed forest. The original fire masks were in an equidistant projection in meters, which we transformed to a WGS84 grid with corresponding latitude and longitude. As previously mentioned, there are several confidence estimates included for every fire pixel. We use only the highest confidence class. This selection reduces the number of active fires but is a necessary measure to ensure that we include only those pixels that we are most confident of being active fires. In a last step, we resampled the data to daily masks and increased the resolution to 1° x 1° with the nearest neighbor method. The resulting binary fire masks indicate if we had an active fire on that day or not.

2.2 Methods

2.2.1 Descriptive Statistics

In a first step, we have a look at the ERA5 forest fire danger data over Europe for the period of 1979-2020. We investigate the seasonal climatological mean and standard deviation of the FWI and the FFMC. Then, we examine the EFDE thresholds and the seasonality of EFDE by plotting the season of highest and second highest occurrence (following Mastrantonas et al. 2021). In addition, the temporal dependence of extreme fire danger events is investigated, where we calculate the percentage of EFDE that occurred since the last EFDE at each grid cell with the intervals of 1, 3, 7, and 15 days. It helps to understand the temporal characteristics of EFDE and its persistency as well as the importance of successive events.

2.2.2 Event-Based Metric Description

The event-based metric used in this thesis can be explained with a classic yes/no contingency table (Figure 2.5). An estimated event is being compared to an observed event on a grid cell basis for each field. In that way, only the local influence is considered. Event-based means that we are interested in the effect of the estimated event on the observed event. The matching of these two events results in a new binary field with 1 = match (hits) and 0 = no match (misses).

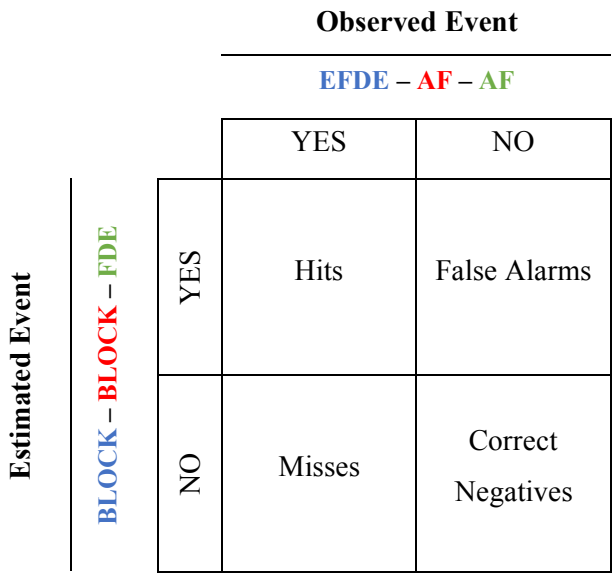

Figure 2.5: Contingency table used for the derivation of different forms of the f -metric used in this master thesis. The verification is based on binary events based on an estimated event and an observed event. EFDE: Extreme fire danger event. FDE: Fire danger event. AF: Active fires. (Figure adapted from Di Giuseppe et al. 2016).

The f-metric, which is the fraction of the hits and the sum of hits and misses in Equation (1), gives an indication on how well the estimated event matches the observed event.

$$f - metric = \frac{Hits}{Hits + Misses} \quad (1)$$

The f-metric can be used to define three metrics that we use in this thesis. As events to estimate, we use atmospheric blocking and fire danger events (FDE) (Figure 2.5). FDE are described in a later section in detail (Chapter 2.2.5) but depict in principle each of the ten percentile ranges of the climatological fire weather danger (>90th, 80th -90th etc.). Thus, FDE describe, depending on the percentile range, all fire danger levels from low to high fire danger. As observed events in the contingency table we utilize EFDE and active fires. The detailed description of each of the three adaptions of the f-metric follows in the next sections.

2.2.3 Blocking and Fire Weather Indices

In this section, we describe how to quantify the relevance of blocking for co-located EFDE closely following the approach of Pfahl and Wernli (2012a). If not stated otherwise, we will use EFDE based on P99. The results for P95 and P97 can be found in the appendix (Figure 6.2 and Figure 6.3). We assume that EFDE are locally related to atmospheric blocking if the grid cell belongs to a block on the respective day. Thus, the hits correspond to the number of EFDE occurring simultaneously with a block at the same location. This is then divided by the total number of fire danger extremes. The co-location percentage f_{EFDE} in Equation (2), which is based on the f-metric define in Equation (1), corresponds to the one used in Pfahl and Wernli (2012b):

$$f_{EFDE} = \frac{N_{block}^{EFDE}}{N_{block}^{EFDE} + N_{no\ block}^{EFDE}}, \quad (2)$$

where N_{block}^{EFDE} denotes the number of EFDE occurring simultaneously with a block at the same location, and $N_{no\ block}^{EFDE}$ indicates the number of EFDE without co-occurring block.

We calculate the co-location percentage f_{EFDE} for the FWI and the FFMC and the ERA5 period of 1979-2020. Furthermore, we calculate an area-weighted regional mean for whole Europe as well as for the four study regions shown in Figure 2.4. We also investigate the large-scale circulation patterns that are present during FWI EFDE at the four study regions.

2.2.3.1 Significance Testing

We assume blocks and co-located fire danger extremes to be unrelated if the percentage f_{EFDE} is equal or similar to the climatological blocking frequency (Figure 2.3). How dissimilar the two must be in order to be significant is determined by a significance test. We use a bootstrap test based on random allocations comparable to the approach of Pfahl and Wernli (2012a). Bootstrapping is a statistical procedure that resamples the original dataset to create many simulated samples. Each simulated sample has its own statistical distribution that can be used to create a confidence interval.

In the following we explain the significance testing step-by-step (following Pfahl and Wernli (2012a)):

(1) First, 500 sample base grid points north of 35°N are selected with average blocking frequencies evenly distributed in the range of the respective seasonal blocking frequency (MAM: 1-16%, JJA: 1-21%, SON: 1-18.5%).

(2) The extreme fire weather danger time series for the matching is selected.

(3) For every of the 500 sample grid points, 1000 event lists of random matches are created. To avoid the selection of grid points near the base grid point and to ensure physical unrelatedness, we remove the grid points in the range ± 90° longitude. Moreover, only land grid points are used for the matching.

(4) In a next step, we match the occurrence of a block at the base grid point with the fire weather danger of a random grid point. In that way, 500 statistical distributions of random matches are created.

(5) The medians of these statistical distributions are plotted against the blocking frequency at the respective base grid point. When the matching frequency and the blocking frequency align the one-to-one line, then blocks and fire extremes are statistically unrelated.

(6) The 1st and 99th percentiles of the distributions as a function of the seasonal blocking frequency are obtained from a quantile regression. These percentiles confine our confidence interval (Figure 2.6)

(7) The relationship between fire extremes and blocks is considered as statistically **not** highly significant when the matching frequency lies within this confidence interval, that is to say, between the two quantile regression lines. Grid points for which the relation is not significant

are masked in white in the results. For the distribution in Figure 2.6 for example, a grid point with a blocking frequency of 10%, the matching frequency would have to be <9% or >12% to be statistically significant.

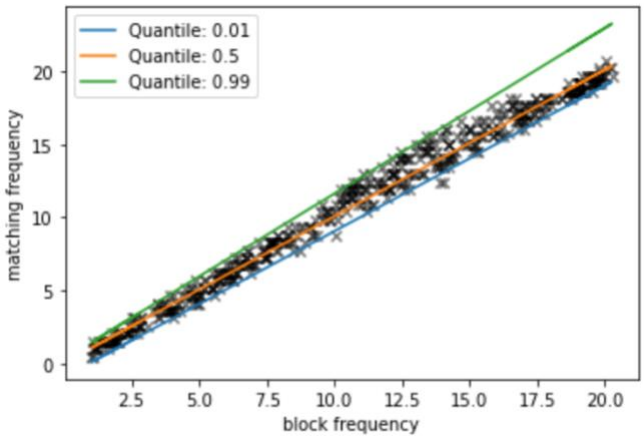

Figure 2.6: An illustrative example of the medians of the 500 statistical distributions (crosses) and the quantile regression lines for the 1st, 50th (median), and 99th percentile level. The green and blue line confine our confidence interval.

Quantile regression is an extension of linear regression analysis (Koenker 2005). Compared to linear regression where we estimate the conditional mean of the response variable, in quantile regression any percentiles can be estimated. In our case, the quantile regression lines go through the estimated 1st and 99th percentile at each level of the predictor variable, which is the blocking frequency (Figure 2.6).

2.2.4 Blocking and Active Fires

We also look at the spatial co-location of atmospheric blocking and active fires. The method is similar to the matching of EFDE with blocks (Chapter 2.2.3). Instead of using EFDE based on the fire weather indices, we take the active fires to match with the blocks. The co-location percentage is highly dependent on how many active fires we have for each pixel. For instance, if there is only one active fire detected at an arbitrary pixel, the co-location percentage attains either a value of 100% if there is a match, or 0% otherwise. Thus, to overcome this bias, we only select pixels with four or more active fires (> 4AF) per season over the period of 1991-2019. The co-location metric f_{AF} is defined as:

$$f_{AF} = \frac{N_{block}^{AF}}{N_{block}^{AF} + N_{no\ block}^{AF}}, \quad (3)$$

where N_{block}^{AF} denotes the number of active fires occurring simultaneously with block at the same location, and $N_{no\ block}^{AF}$ indicates the number of active fires without co-occurring block.

2.2.5 Fire Weather Index and Active Fires

The fire weather indices of ERA5 describe a potential fire danger, which means that high values indicate the probability of spontaneous ignition, but do not guarantee the occurrence of an actual fire (Di Giuseppe et al. 2016). For fire action planning it is desirable that the FWIS can discriminate between a real fire occurrence and a nonevent. This is a difficult task for any weather extremes, but especially challenging for fire events since the ignition source is impossible to predict. The reason is that the majority (above 95%) of forest fires are ignited by humans, both due to arson and negligence (de Rigo et al. 2017, Ganteaume et al. 2013). Thus, to quantify the performance of the FWIS, one can calculate different measures of a dichotomous forecast from a contingency table (Figure 2.5). In this thesis, we validate the FWI with active fire masks derived from satellite data. It is important to state that we do not use FWI forecasts here but rather FWI reanalysis data, which will be referred to as an estimation of a fire event. Reanalysis data incorporates observation and is thus a retrospective estimation of the fire weather danger and not a prediction of the future fire danger. However, by using reanalysis fire weather indices we can assess the potential predictability of the modeling components in the forecasting system and where they could provide useful information for fire management (Di Giuseppe et al. 2016).

In order to validate the estimated FDE and how good they match the observed active fires, we calculate the probability of detection (POD), which we define as the metric f_{POD}. The metric f_{POD}, also called the hit rate, is calculated as follows:

$$f_{POD} = \frac{N_{FDE}^{AF}}{N_{FDE}^{AF} + N_{no\ FDE}^{AF}}. \quad (4)$$

In Equation (4), N_{FDE}^{AF} indicates the number of active fires occurring simultaneously with an FDE at the same grid cell, whereas $N_{no\ FDE}^{AF}$ denotes the number of active fires without co-occurring FDE. We use FDE instead of EFDE, since we want to assess, which FWI range matches the active fires best. Thus, we divide the FWI into ten percentile ranges in steps of 10 (>90th, 80th-90th etc.), which are all FDE with different fire danger. In this way, we can look at which percentile range matches the real fire occurrence best. The percentiles can be defined based on the yearly distribution or on the seasonal distribution of the FWI. However, the former introduces a bias towards the summer season as there are more days with higher FWI values in summer. For this reason, we mainly use the seasonal percentile definition for our analysis. Nevertheless, we also calculate the f_{POD} with the FWI percentile ranges calculated based on the yearly distribution to be able to compare the results with previous findings (Di Giuseppe et al. 2016,

Di Giuseppe et al. 2020). We calculate the f_{POD} for every grid cell and the period of 1991-2019. Furthermore, we calculate an area-weighted regional mean f_{POD} for whole Europe as well as for the four study regions (Figure 2.4). We also calculate a seasonal mean of the probability of detection f_{POD} for entire Europe.

The f_{POD} is a good measure for rare events but is very sensitive to the climatological frequency of the event. It has a range of possible values of 0 to 1, where a perfect score would be 1 as then 100% of the observed events were detected correctly. The f_{POD} has been used before with observed fires and forecasts of FWI (Di Giuseppe et al. 2020), as well as with FWI reanalysis data (Di Giuseppe et al. 2016).

2.2.6 BIAS Score

In order to understand the frequency bias of our estimated and observed events we calculate the BIAS score:

$$BIAS = \frac{Hits + False\ Alarms}{Hits + Misses} = \frac{N_{FDE}^{AF} + N_{FDE}^{no\ AF}}{N_{FDE}^{AF} + N_{no\ FDE}^{AF}}, \quad (5)$$

where $N_{FDE}^{no\ AF}$ indicates the number of FDE without co-occurring active fire and the others correspond to the ones used in Equation (4). This frequency bias simply measures the ratio of the frequency of estimated events by the FWI to the frequency of observed active fire events. The BIAS score indicates if the FWI system has the tendency to underestimate (BIAS < 1) or overestimate (BIAS > 1) active fire events.

3 Results

3.1 Case Study Summer 2018

The summer of 2018 was amongst the hottest European summers on record, with large parts of Scandinavia and Central Europe affected by heatwaves (Spensberger et al. 2020). These unusually hot and dry conditions led to a large number of wildfires, which is why the summer of 2018 serves as an ideal case study for this thesis. In this chapter, we investigate the spatial and temporal variability of several fire weather indices and the influence of the large-scale circulation over Europe in 2018. We also examine monthly blocking occurrence and the active fire occurrence for the year 2018 to understand how blocks, FWI and active fires are linked. Thus, our goal is to illustrate the potential role of blocks on the occurrence and spatiotemporal variability of high fire weather danger and active fires. Since Scandinavia suffered from unprecedented wildfires, we lay a special focus on Northern Europe in this case study.

In Figure 3.1, the monthly FWI percentile ranking indicates whether the fire weather danger is below average (blue), near average (white), or above average (red). For example, if a pixel is colored in dark red, 2018 is the year with the highest fire weather danger climatologically. In June, the fire weather danger is especially high around the Baltic Sea and Great Britain, while it is near average in Central Europe and below average in Southern Europe (Figure 3.1a). At the same time, we observe a weak ridge over the Faroe Islands and a low-pressure anomaly is located over the Iberian Peninsula. Only a few active fires are detected throughout Europe in June. In July, Northern Europe exhibits extreme fire weather danger as well as Great Britain and parts of Central Europe.

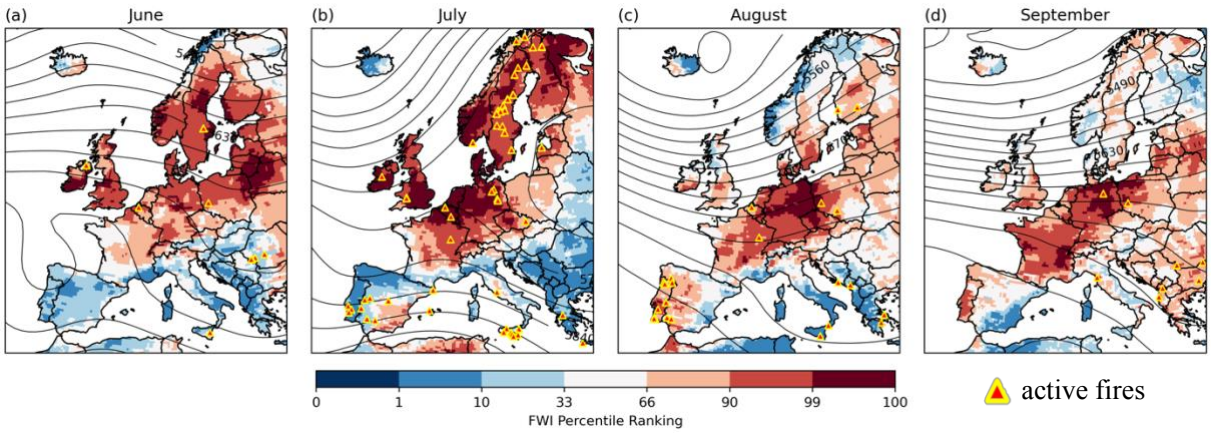

Figure 3.1: Monthly fire weather danger of the FWI (percentile ranking, shading) for the months JJAS in 2018 compared to 1979-2020, monthly mean 500-hPa geopotential height (Z500) (in m, black contours), and active fires (only forest fires and high confidence).

The upper-level circulation pattern indicates a ridge regime with a blocking over Northern Europe (Figure 3.1b). Based on the Z500 contours, the flow over Europe is split and diverted meridionally far to the north around the block. There are a lot of active fires in Sweden, as well in Central Europe, the Iberian Peninsula and Sicily. In Northern Europe, the active fires occur co-located with high fire weather danger and increased geopotential height, while in Southern Europe, active fires occur in regions with below average fire weather danger. In August, the FWI ranks high in Central Europe and Portugal, where also a lot of active occur. The upper-level geopotential height indicates a zonal regime in August that continues into September (Figure 3.1c and d). In September, the fire weather danger is still high in Germany and parts of Western Europe with a few active fires.

To further understand the temporal behavior of the Canadian fire weather indices at the onset and throughout the extremely hot and dry summer of 2018, we look at standardized mean time series of the indices averaged over Europe and Northern Europe only (Figure 3.2). Figure 3.2a shows the temporal evolution of the three moisture codes (FFMC, DMC, and DC) for whole Europe. The FFMC shows a large day-to-day variability and increases earlier than the other indices, an expected behavior since it describes the fuel moisture of the litter that reacts quickly to changing environmental conditions. This is followed by an increase of the DMC, which describes the moisture in the second layer. The DC, the most inert index due to its lag of 52 days, increases with the slowest rate. The FFMC stays on a relative high level of 1σ with strong fluctuations from April to September, while the DMC and DC peak in late summer and exhibit a smoother evolution.

For Northern Europe, the FFMC displays a similar pattern as for whole Europe but with even greater variability (Figure 3.2b). The DMC shows two steep rises, one in May and one in July, which peak at above 2σ in early June and late July, respectively. Those two peaks are only slightly visible in the FFMC. For the DC, we see a continuous increase and only one peak in July, as the moisture information accumulates over time.

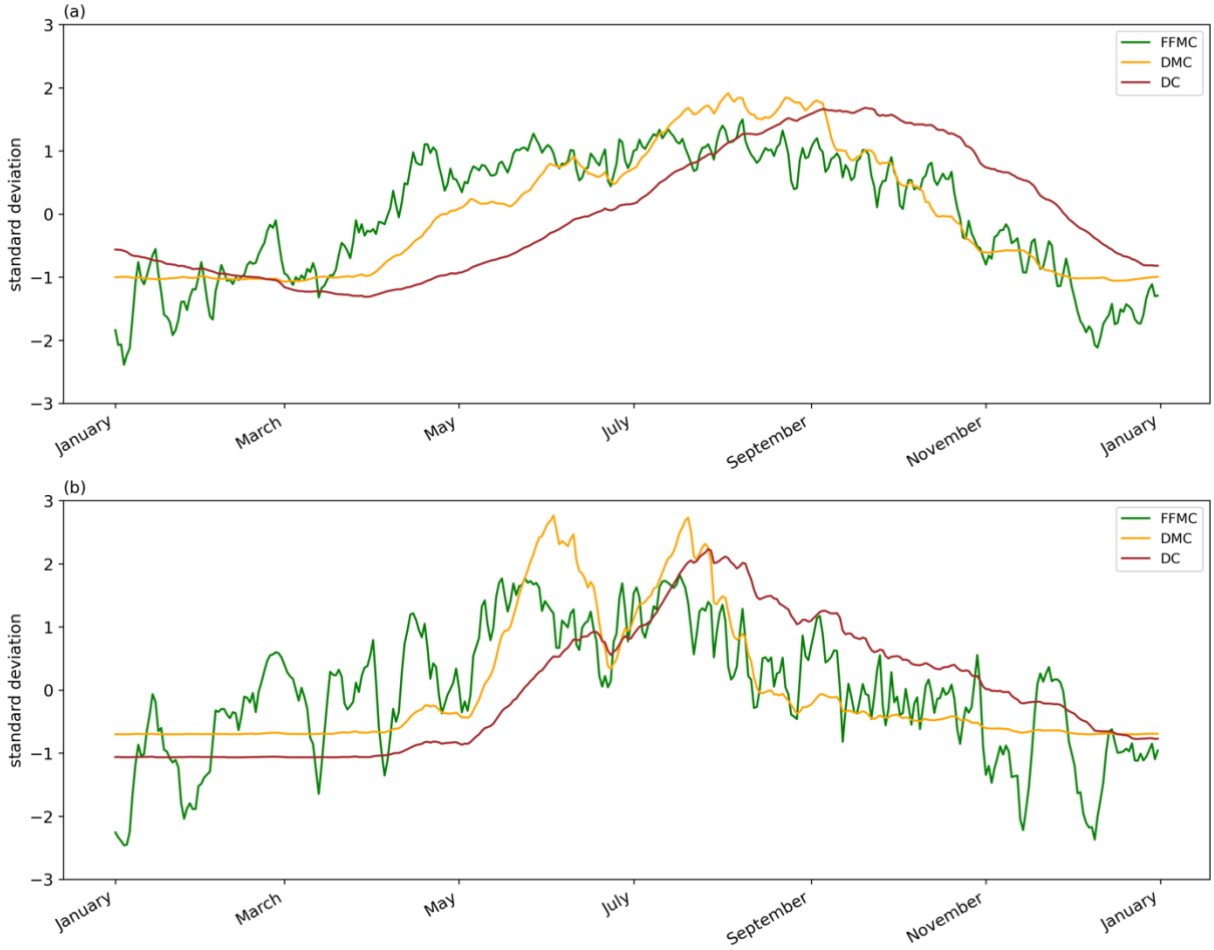

Figure 3.2: Temporal evolution of the area-weighted and standardized mean of the three fuel moisture codes, FFMC, DMC and DC, for (a) Europe and (b) Northern Europe in 2018.

To obtain a complete picture, we show in Figure 3.3 the temporal evolution of the three fire behavior indices (BUI, ISI and FWI). Averaged over Europe, we see an almost synchronous evolution of the BUI, ISI and FWI (Figure 3.3a). The black line (BUI) has the strongest lag of the three indices, since it is a weighted combination of the DC and DMC. The ISI combines the FFMC and wind speed and thus shows a similar high daily variation as the FFMC. The FWI, which combines the BUI and ISI, contains the information from all indices. Around April, the indices start to rise at different rates and with different daily variabilities. During the course of the year, the three indices show some local peaks in June and July and reach their maximum level in late summer. From September onwards, the indices start to decrease again to lower levels of fire weather danger.

For Northern Europe, however, the ascent of fire weather indices is much steeper. Two distinct high points with a magnitude of 3σ, as seen before for the DMC (Figure 3.2b), are apparent for all three behavior indices (Figure 3.3a). This strong deviation from the mean (3σ) matches the extremely high fire danger ranking in June and July (Figure 3.1a and b).

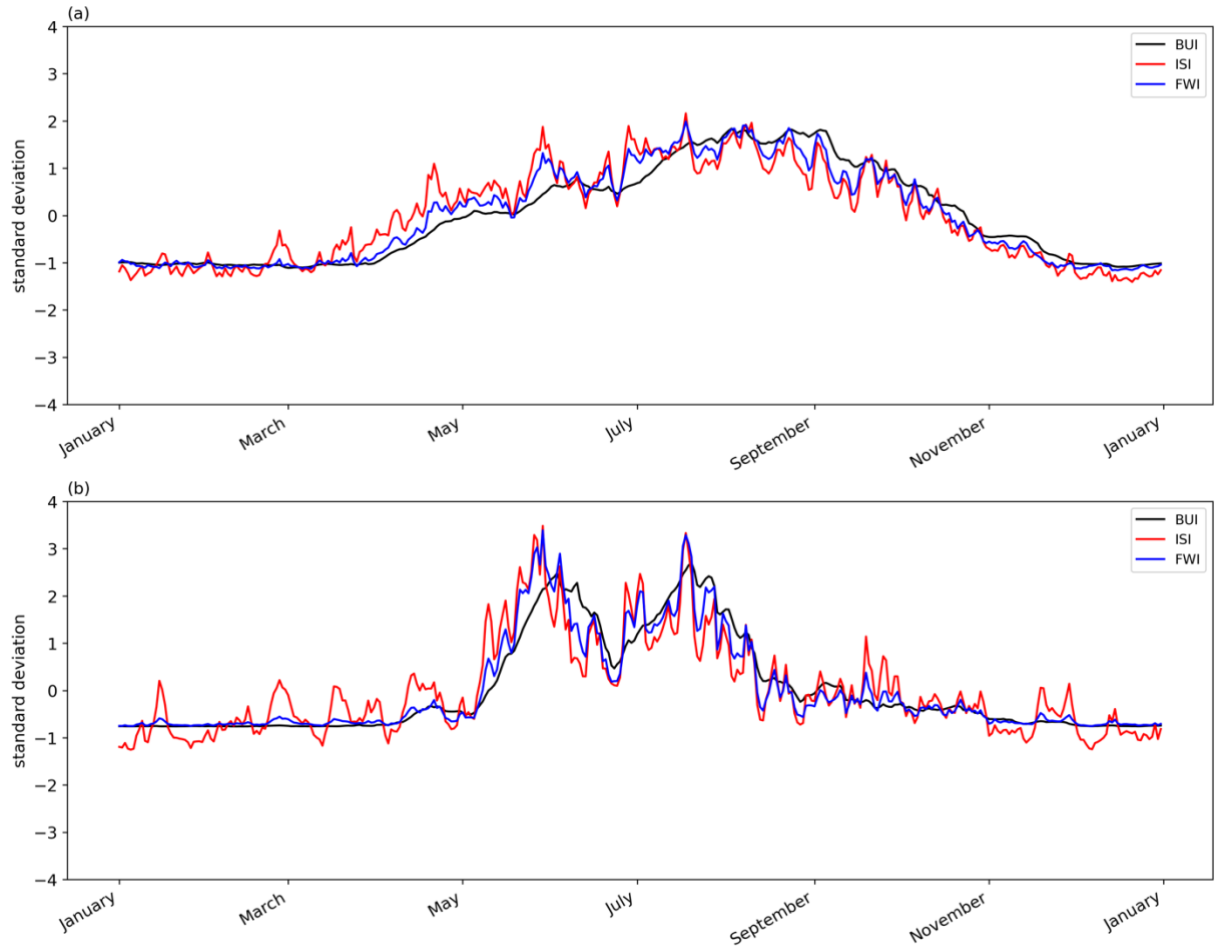

Figure 3.3: Temporal evolution of the area-weighted and standardized mean of the three fire behavior indices, BUI, ISI and FWI, for (a) Europe and (b) Northern Europe in 2018.

To investigate the cause of these two peaks in June and July, we look at the influence of atmospheric blocking on the fire weather danger. In Figure 3.1b, we see that a blocking pattern is visible in the Z500 in July. In a next step, we look at the monthly blocking frequencies of 2018. Figure 3.4a shows on how many days there is a block present over each grid cell, with 100% indicating that a block was present on every single day of the month. The first three months in 2018 do not have high blocking frequencies over Europe with values below 20%. In April, the blocking frequency reaches values of 20-40%. In May, there is a considerable block (up to 70%) centered over Scandinavia, whereas in June highest blocking frequencies are shifted towards the North Atlantic. In July, Northern Europe is again under the influence of atmospheric blocking with values up to 70%. In August and September, the blocking frequency over Europe is again lower with values mostly below 30%.

The pronounced blocking patterns in May and July over Northern Europe and over the North Atlantic in June of 2018 (Figure 3.4a) lead to extremely high fire danger over Scandinavia (May and June) and Great Britain (June) (Figure 3.1a-c). The temporal evolution of the blocking frequency in Northern Europe (Figure 3.4b) correlates well with the fire weather indices in summer but not in winter (Figure

3.2b and Figure 3.3b). Blocks in winter (February and November) do not influence most indices, only the FFMC and the ISI increase a little. Thus, we conclude that blocks in summer over Northern Europe occur simultaneously with extreme fire weather danger. In a later chapter (3.3), we will quantify the relevance of blocking for extreme fire weather danger.

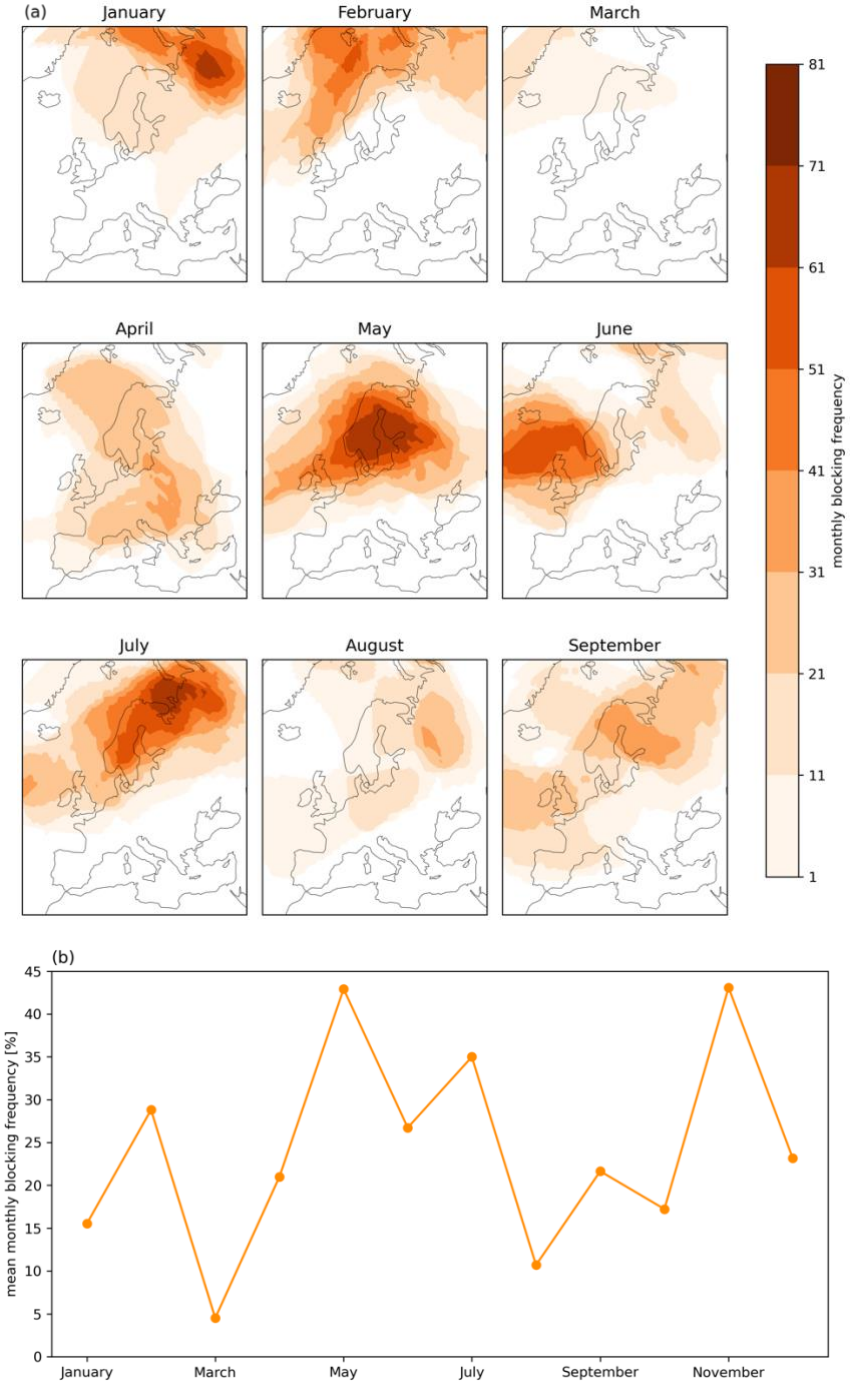

Figure 3.4: (a) Monthly relative blocking frequency (in %) for Europe in 2018 and (b) Temporal evolution of the area-weighted mean of the monthly relative blocking frequency for Northern Europe in 2018.

3.2 Descriptive Statistics

To investigate the spatiotemporal variability of fire weather danger, we look at the seasonal climatological mean and standard deviation of the FWI and FFMC (Figure 3.5-3.8). Then, the thresholds for EFDE give an indication of how high the most extreme fire weather danger days are in the respective seasons (Figure 3.9 and Figure 3.10). We also examine the seasonality of the occurrences of EFDE as well as the temporal dependence of EFDE (Figure 3.11 and Figure 3.12).

The seasonal mean climatology for the FWI shows a strong spatial and temporal variability with a strong north-south gradient (Figure 3.5). The highest mean FWI values occur in the summer season and in Southern Europe. Especially on the Iberian Peninsula, the mean fire weather danger is very high during the summer months with mean FWI values above 32. In Northern Europe, the fire weather danger is low most of the time, which is reflected in the low values below 8. Central Europe is a transition zone with average mean fire weather danger in all season but DJF when it is below 1.

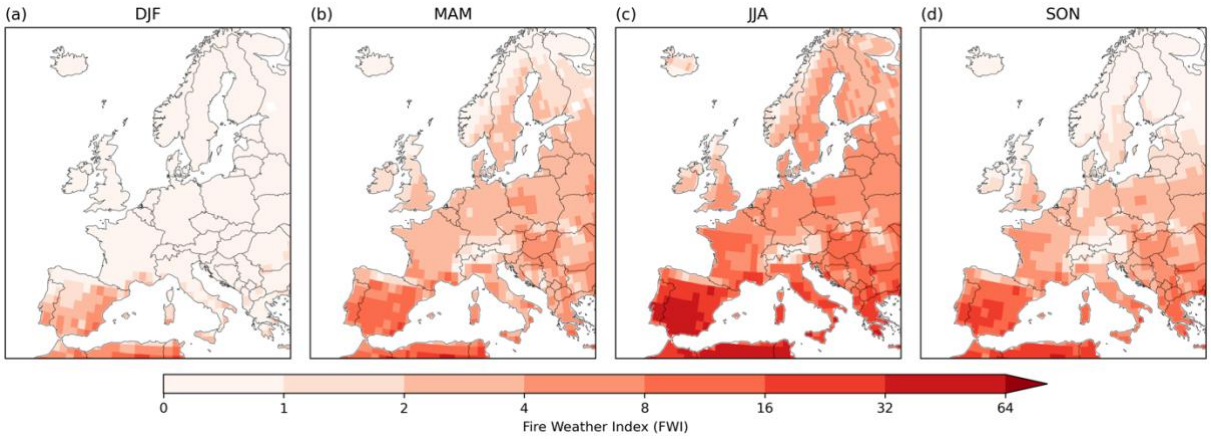

Figure 3.5: Seasonal climatological mean of the FWI fire weather danger for all years in the ERA5 period (1979-2020).

In Northern Europe, the distribution of FWI values is right-skewed (not shown), resulting in small standard deviations of 8 in summer and below 1 in the other seasons (Figure 3.6). In Southern Europe, the FWI distribution is more left-skewed (not shown), and the standard deviation is high with up to 32. Throughout Europe, the summer months exhibit the greatest spread with FWI deviations ranging from 2 in Northern Europe and 32 in Southern Europe, followed by spring and autumn. In the corresponding discussion section (Chapter 4.2) we discuss what these values mean.

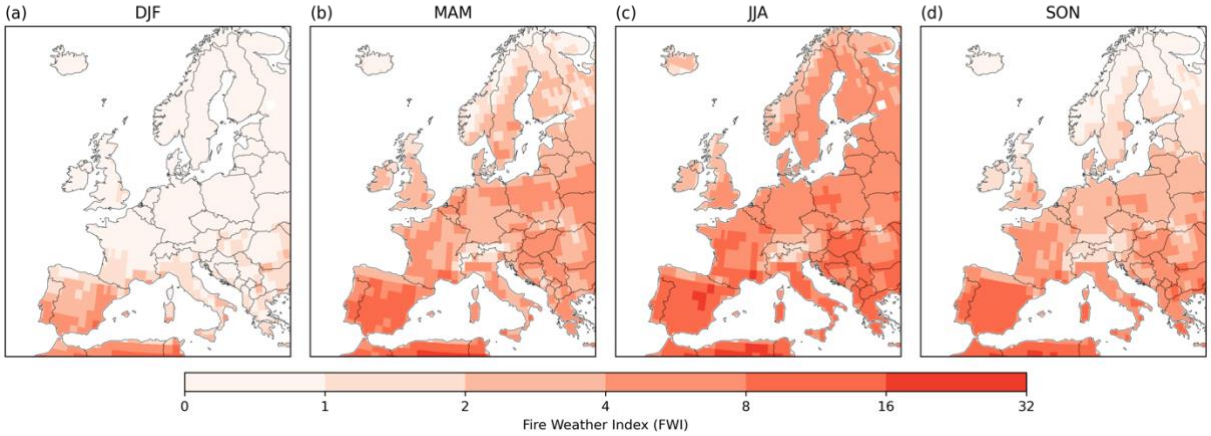

Figure 3.6: Seasonal climatological standard deviation of the FWI fire weather danger for all years in the ERA5 period (1979-2020).

Similar to the FWI, the FFMC shows the driest fuel moisture conditions also in summer and in Southern Europe (Figure 3.7). In all regions of Europe, the mean FFMC never falls to near zero values. In Northern Europe, the FFMC mean reaches values of about 50 in winter and up to 70 in spring and summer, which correspond to dry fuel moisture conditions. In Southern Europe, the mean FFMC is dry throughout the year with extreme values exceeding 85 in summer. The FFMC is the only component of the Canadian FWIS that has no open-ended scale (maximum = 99), which emphasizes that the FFMC reaches very high values on average, especially in summer (Van Wagner 1987).

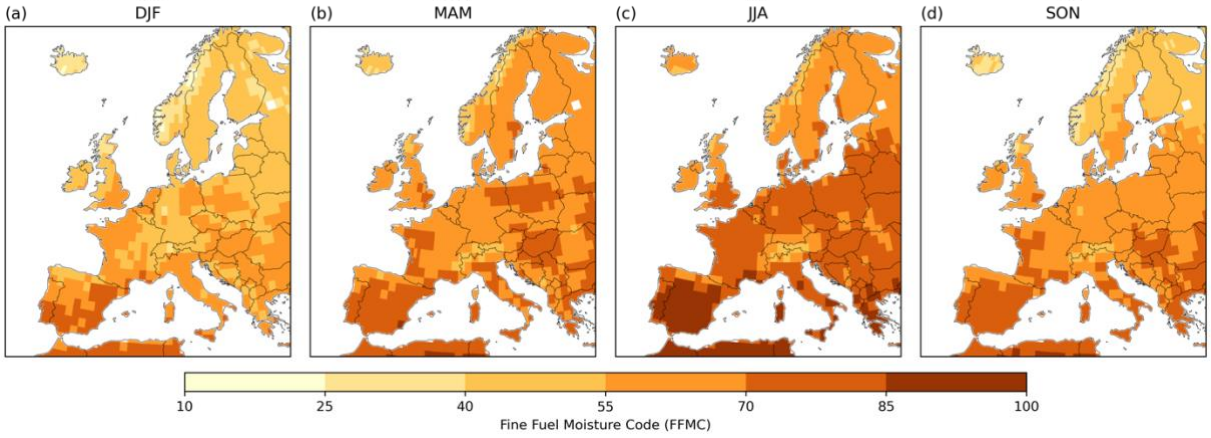

Figure 3.7: Seasonal climatological mean of the FFMC fire weather danger for all years in the ERA5 period (1979-2020).

Figure 3.8 shows that the FFMC standard deviation is small in Southern Europe in summer. This stands in contrast to the FWI, where we had the largest standard deviation in summer (Figure 3.6). In Northern Europe, the FFMC variability is highest with daily standard deviations of up to 25 in summer and

autumn, and around 20 in winter. Spatially, winter and spring show a very similar pattern across Europe. In contrast to the FWI, the Alps exhibit very high FFMC standard deviation values in all seasons.

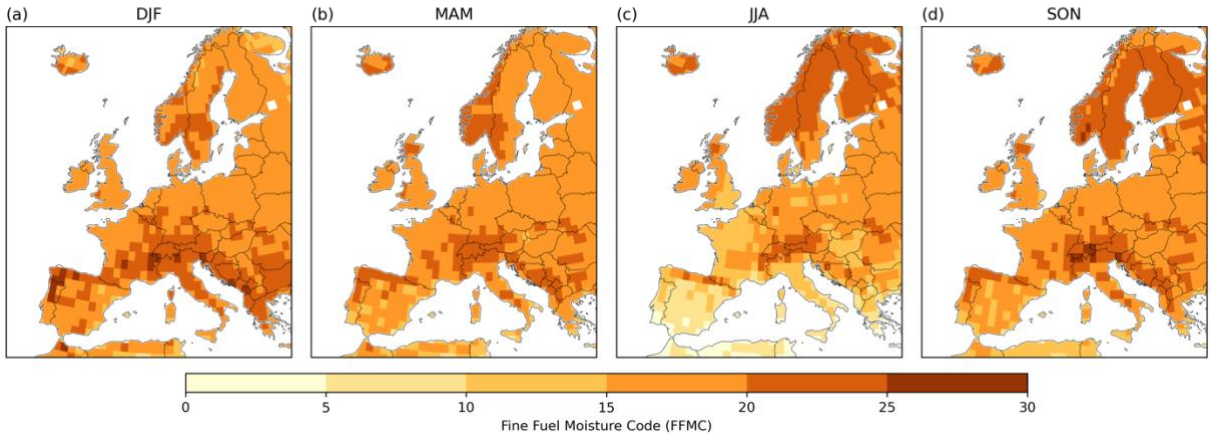

Figure 3.8: Seasonal climatological standard deviation of the FFMC fire weather danger for all years in the ERA5 period (1979-2020).

The EFDE thresholds (defined seasonally on the 99th percentile of all days for every grid cell) give an indication of how high the most extreme fire weather danger days are in the respective seasons (following Pfahl and Wernli 2012a). The 99th percentile of all available days corresponds to 39 days per season, on which the indicated FWI threshold is being exceeded. Thus, one can say that the higher the threshold, the more extreme the fire weather danger for that specific grid cell. From here, we focus on the three seasons spring, summer, and autumn, since fire weather danger in winter is negligible according to the mean FWI and FFMC (Figure 3.5 and 3.7). We use the fire danger classes from the European Forest Fire Information System (EFFIS) in order to examine to which category the EFDE thresholds belong. In June 2021, a 'Very Extreme' fire danger class (FWI >= 70) was introduced in order to discriminate events in areas that were classified as 'Extreme' mainly in the Mediterranean during summer (EFFIS n.d.).

Figure 3.9 shows that the thresholds are highest in Southern Europe (especially on the Iberian Peninsula) and around the Black Sea. In the Scandinavian Mountains, in the Alps, and in the Carpathian Mountains the thresholds are the lowest. The summer season displays the most extreme fire weather danger throughout Europe. In Northern Europe, the lowest FWI thresholds occur in autumn in the lowest danger class with below 5.2. In Southern Europe, on the other hand, the lowest values occur in spring, but still in moderate to extreme danger classes.

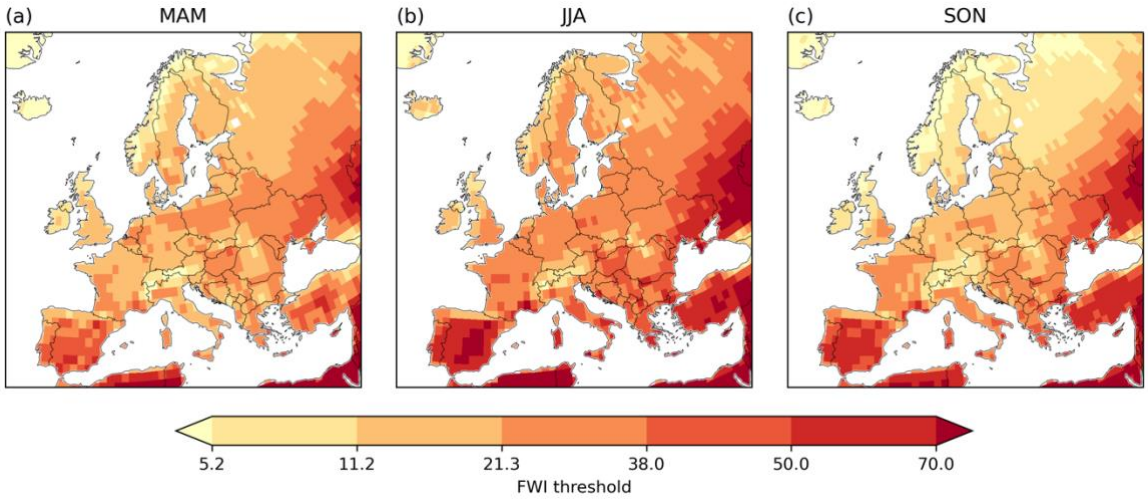

Figure 3.9: The 99th percentile of the daily maximum fire weather danger (FWI thresholds) for each season and for the ERA5 period (1979-2020). The FWI fire weather danger is mapped based on the 7 EFFIS danger classes (Very Low, Low, Moderate, High, Very High, Extreme and Very Extreme).

The FFMC threshold map (Figure 3.10) shows a similar spatial pattern to the FWI with highest values in Southern Europe. However, for the FFMC we have much higher threshold values than for the FWI, which corresponds to the higher mean climatology of the FFMC (Figure 3.7). In summer, many regions such as Southern and Western Europe as well as around the Black Sea exhibit values in the highest FFMC danger class. The seasonal variation is very similar to the FWI with highest values occurring during summer months. The lowest FFMC thresholds appear in autumn throughout Europe.

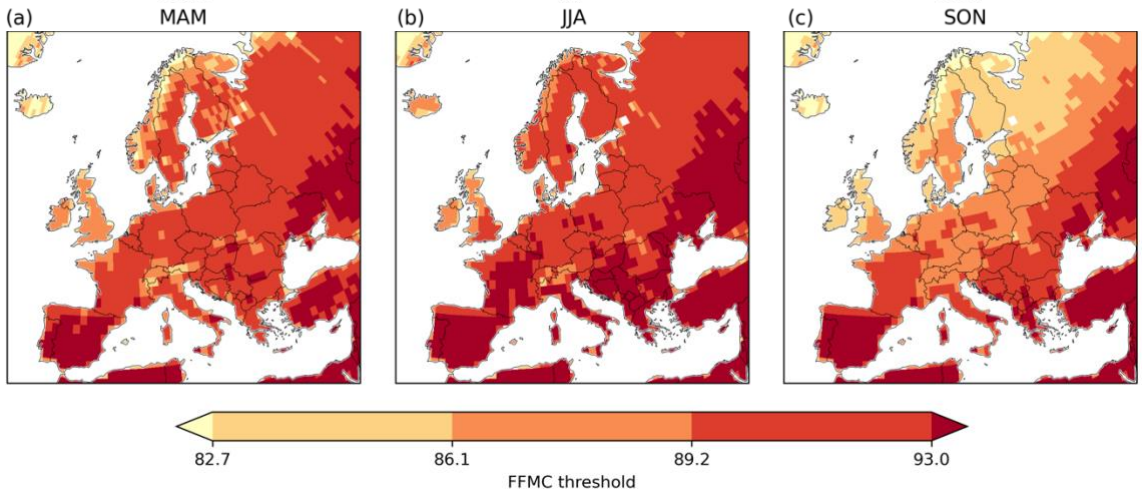

Figure 3.10: The 99th percentile of the daily maximum fire weather danger (FFMC thresholds) for each season and for the ERA5 period (1979-2020). The FFMC fire weather danger is mapped based on the 5 EFFIS danger classes (Very Low, Low, Moderate, High and Very High).

In this section, we focus on the seasonality of EFDE for the FWI, which is very similar to the FFMC (not shown). In Figure 3.11, we see that most EFDE occur in summer across Europe. In Northern and Central Europe, the second most EFDE occur in spring, while in Western and Southern Europe it is in autumn. Thus, both the mean climatologies and the EFDE occurrence indicate that the fire weather danger is lowest in winter (Figure 3.5, Figure 3.7 and Figure 3.9). Therefore, in our analyses we focus on the three seasons spring, summer, and autumn.

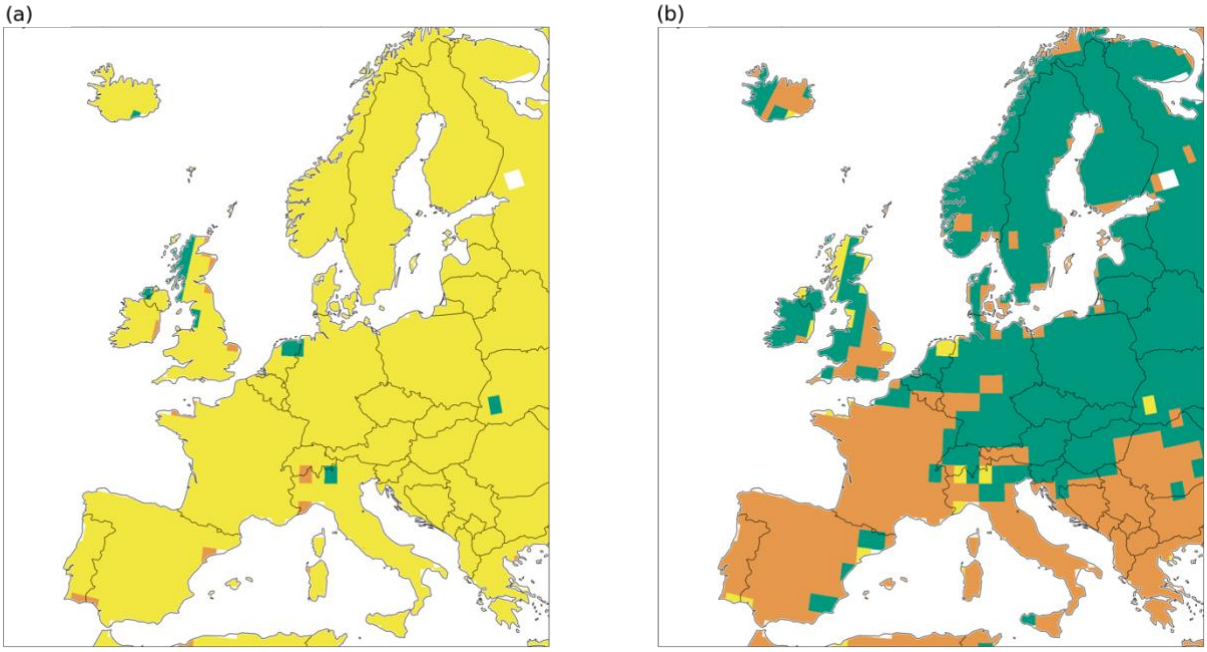

Figure 3.11: Season of (a) highest and (b) second highest occurrence of FWI EFDE (P99) at each grid cell and for the ERA5 period (1979-2020). The colors represent in Green: MAM, Yellow: JJA, Brown: SON.

Figure 3.12 shows the temporal dependence of EFDE in four different time intervals and for summer. In Europe, the percentage of EFDE occurring within 1 day or 3 days following a preceding EFDE is about 37% and 47%, respectively (medians of all grid cells). It increases up to 55% and 63% for an interval of 7 days or 15 days, respectively. This corresponds to almost 2/3 of all EFDE occurring within two weeks of a previous EFDE. Spatially, it is noticeable that the temporal dependence of EFDE is generally higher in Northern Europe and Central Europe compared to Southern Europe (especially the Iberian Peninsula) for every time interval. This means that for an arbitrary EFDE at a grid cell in Sweden, there is a higher probability for another EFDE to occur within the next few days compared to a grid cell in Spain. On the Iberian Peninsula, more isolated EFDE seem to occur according to the low temporal dependence. In the discussion (Chapter 4.2), these results will be discussed in detail.

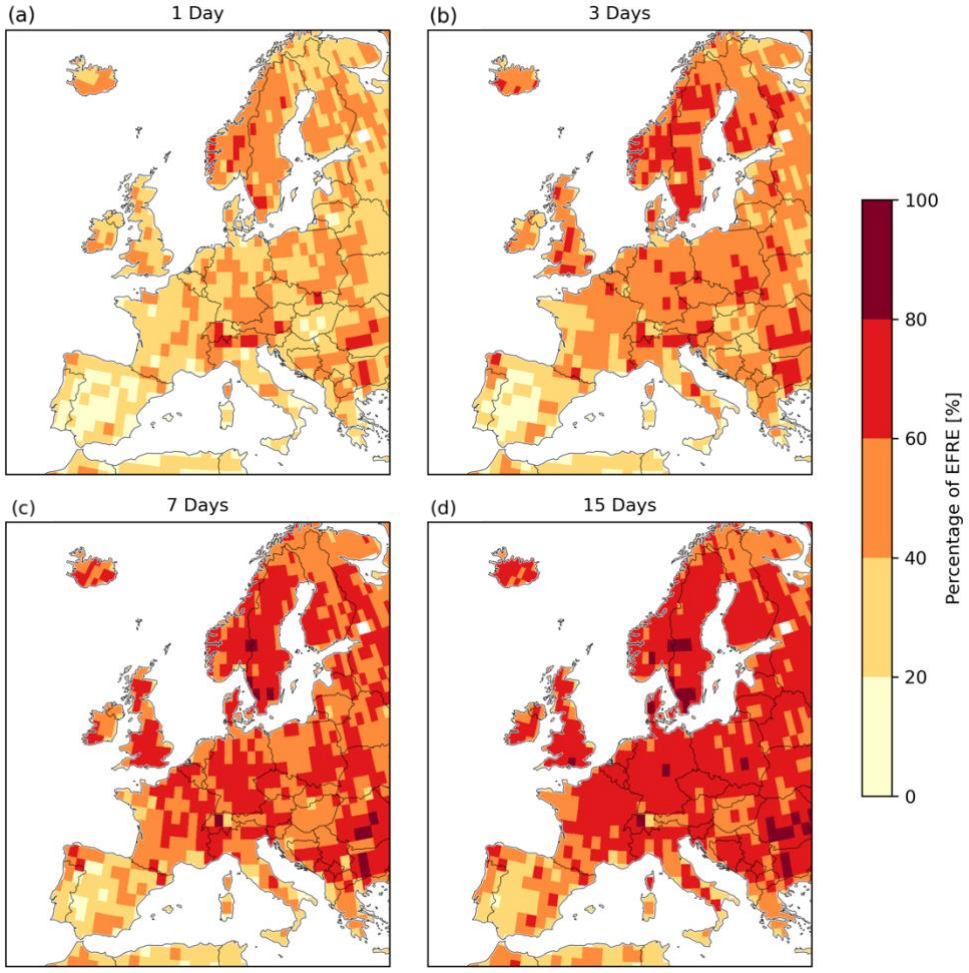

Figure 3.12: Temporal EFDE dependencies indicating the percentage of EFDE that occur within the selected temporal intervals (a: 1 day; b: 3 days; c: 7 days; d: 15 days) from a preceding EFDE at the same grid cell in JJA.

Before we analyze the link between blocking and EFDE in the following chapter, we describe shortly the seasonal blocking frequency for Europe (Figure 2.3). The seasonal blocking frequencies indicate that blocking occurs more often over Northern Europe than Southern Europe. In winter, the maximum blocking frequencies occur over the North Atlantic, while in the other seasons they are found over Scandinavia. The highest occurrence of blocks in Northern Europe appears in autumn followed by summer with 15% and more. In Southern Europe, blocking frequencies of 1-3% occur mainly in spring and autumn.

3.3 Blocking and Fire Weather Indices

The case study of the very hot summer of 2018 (Chapter 3.1) demonstrated that very high fire weather danger in Northern Europe occurred simultaneously with blocks. In order to investigate the role of atmospheric blocking as a potential driver of the spatiotemporal variability of extreme fire weather danger during 1979-2020, in this chapter we quantify the relevance of blocking for EFDE with the co-location percentage f_{EFDE}.

Figure 3.13 shows the percentage f_{EFDE} of EFDE that occur co-located with atmospheric blocking at the same location during the period of 1979-2021. In general, the FFMC shows higher f_{EFDE} values (Figure 3.13d-f) than the FWI (Figure 3.13a-c) for all seasons. In summer, the f_{EFDE} reaches maxima of over 80% for the FWI (Figure 3.13b) and 100% for the FFMC (Figure 3.13e). In Northern Europe and European Russia, the f_{EFDE} for the FWI reaches values of over 70-80%, in Central Europe between 10-30% and in Western Europe up to 50% (Figure 3.13a-c). This means that in Northern Europe, about 7-8 out of 10 FWI EFDE occur with a co-located block in summer. In Southern Europe, the f_{EFDE} attains values of below 30% in all seasons.

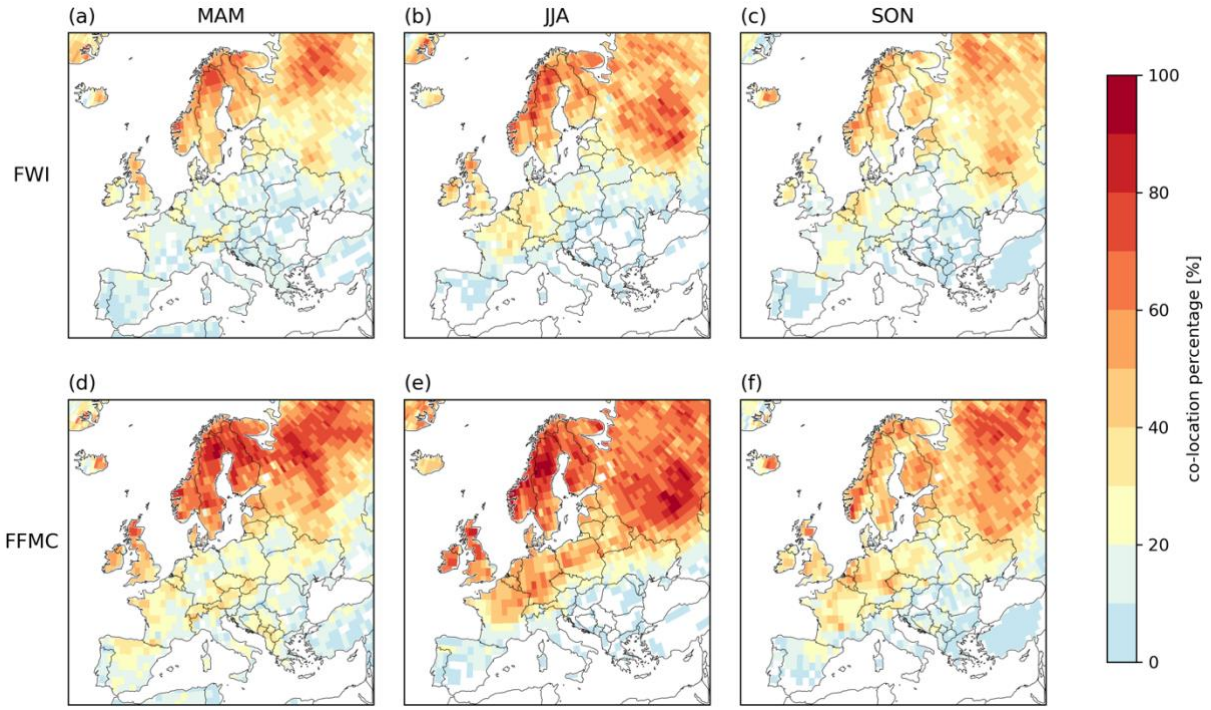

Figure 3.13: Percentage f_{EFDE} of extreme (P99) fire weather danger events (EFDE) occurring simultaneously with a blocking event at the same location for (a, d) spring, (b, e) summer and (c, f) autumn and for (a-c) the FWI and (d-f) the FFMC during 1979-2020. Non-significant grid points are masked in white (based on a bootstrap method and a 99% confidence level). (See Appendix for P95 and P97 (Figure 6.2 and Figure 6.3)).

The f_{EFDE} for the FFMC reaches values of 90-100% in Northern Europe and European Russia, 30-60% in Central Europe and in Western Europe up to 70% (Figure 3.13d-f). Figure 3.13 shows that in summer the f_{EFDE} in Northern and Central Europe reaches the highest values, followed by spring and autumn. In Southern Europe, the highest f_{EFDE} occur in spring followed by autumn and in summer it is the lowest.

Pfahl and Wernli (2012a) investigated the percentage f of warm temperature extremes co-located with blocking. They describe that the percentage f should be compared to the seasonal blocking frequency. Thus, we also compare the percentage f_{EFDE} to the seasonal blocking frequencies (Figure 2.3). In all regions where blocking often occurs, which includes large parts of Northern Europe, the f_{EFDE} for the FWI exceeds the seasonal blocking frequencies by about a factor of 4-5. For the FFMC, the exceedance of the f_{EFDE} over the relative blocking frequency is similar to the FWI but increases up to a factor of 6-8 in western Russia in summer (Figure 3.13e). In contrast to the relative blocking frequency, where the highest values occur in autumn over Northern Europe (Figure 2.3), we have the highest co-location percentages in the summer season for both indices (Figure 3.13b and e). Given that the f_{EFDE} is many times higher than the seasonal blocking frequencies in Northern and Western Europe indicates a strong and statistically significant relationship between EFDE and co-located atmospheric blocking, as demonstrated with the bootstrap method.

The lagged analysis, where we incorporate the blocking information of the past week, yield a similar spatial pattern as in Figure 3.13 but with higher FWI values in summer and similar or lower values in spring and autumn (not shown). In general, the lagged f_{EFDE} is high in summer for Scandinavia and Great Britain. The lagged f_{EFDE} values for the FFMC are lower in every region and season.

3.3.1 Regional Analysis

To better compare different regions, we calculate the regional area-weighted means of f_{EFDE} for the four European study regions defined in Figure 2.4, and the values are listed in Table 3.1. In the two Mediterranean regions, the highest mean f_{EFDE} for FWI occur in spring with around 10%. In contrast, in Central and Northern Europe the FWI maxima appear in the summer season with averages of 25-41%. For the FFMC, we have an average f_{EFDE} of 17-19% in Southern Europe in spring and in summer up to 40% and 58% in Central Europe and Northern Europe, respectively.

*Table 3.1: Regional area-weighted mean of f_{EFDE} (in %) for the FWI and FFMC for the four study regions and whole Europe. The numbers in **bold** are mentioned in the text.*

	FWI			FFMC		
	MAM	JJA	SON	MAM	JJA	SON
Eastern Mediterranean	**10.2**	3.7	5.5	**16.8**	5.4	8.7
Western Mediterranean	**10.6**	6.6	8.1	**19.2**	10.0	12.5
Central Europe	18.2	**24.5**	22.2	27.8	**40.3**	30.2
Northern Europe	39.3	**41.0**	33.6	53.8	**58.1**	41.3
Europe	19.6	19.0	17.4	29.4	28.4	23.2

In addition to the grid-by-grid co-location analysis (Figure 3.13), we investigate the large-scale circulation patterns during EFDE in the four study regions in Europe. In Figure 3.14 we show composites of the synoptic situation during FWI EFDE in summer, which includes relative blocking frequencies and Z500 anomalies. The relative blocking frequency is calculated based on the total EFDE days. The Z500 anomalies are defined as the difference of the Z500 during the EFDE and the seasonal averaged Z500.

In Northern Europe, as expected, the blocking frequencies are high with up to 75% since it is the region where we found high co-location percentages (Figure 3.13 and Figure 3.14). For EFDE in Central Europe, the blocking frequency is lower with maxima of 50-60% and a pronounced positive Z500 anomaly is located over the Baltic Sea. Figure 3.13 reveals that the co-location percentages are low in Southern Europe, due to the low blocking frequencies. For this reason, we want to investigate which upper-level circulation patterns are important when the fire weather danger is high also in Southern Europe.

For the two Mediterranean regions, the *in-situ* blocking frequencies are low; only over the North Atlantic do the values reach around 30%. Instead, a subtropical ridge appears in the composite of the Z500 anomalies for both the Western Mediterranean and the Eastern Mediterranean region. In both cases, the ridge axis is shifted to the north-east with respect to the study boxes. Upstream of the subtropical ridge, there is an upper-level trough with its axis located over the North Atlantic near the Celtic Sea for Western Mediterranean and over the North Sea and the Norwegian Sea for Eastern Mediterranean. Composites of absolute Z500 during EFDE for the four study regions can be found in the Appendix (Appendix Figure 6.4).

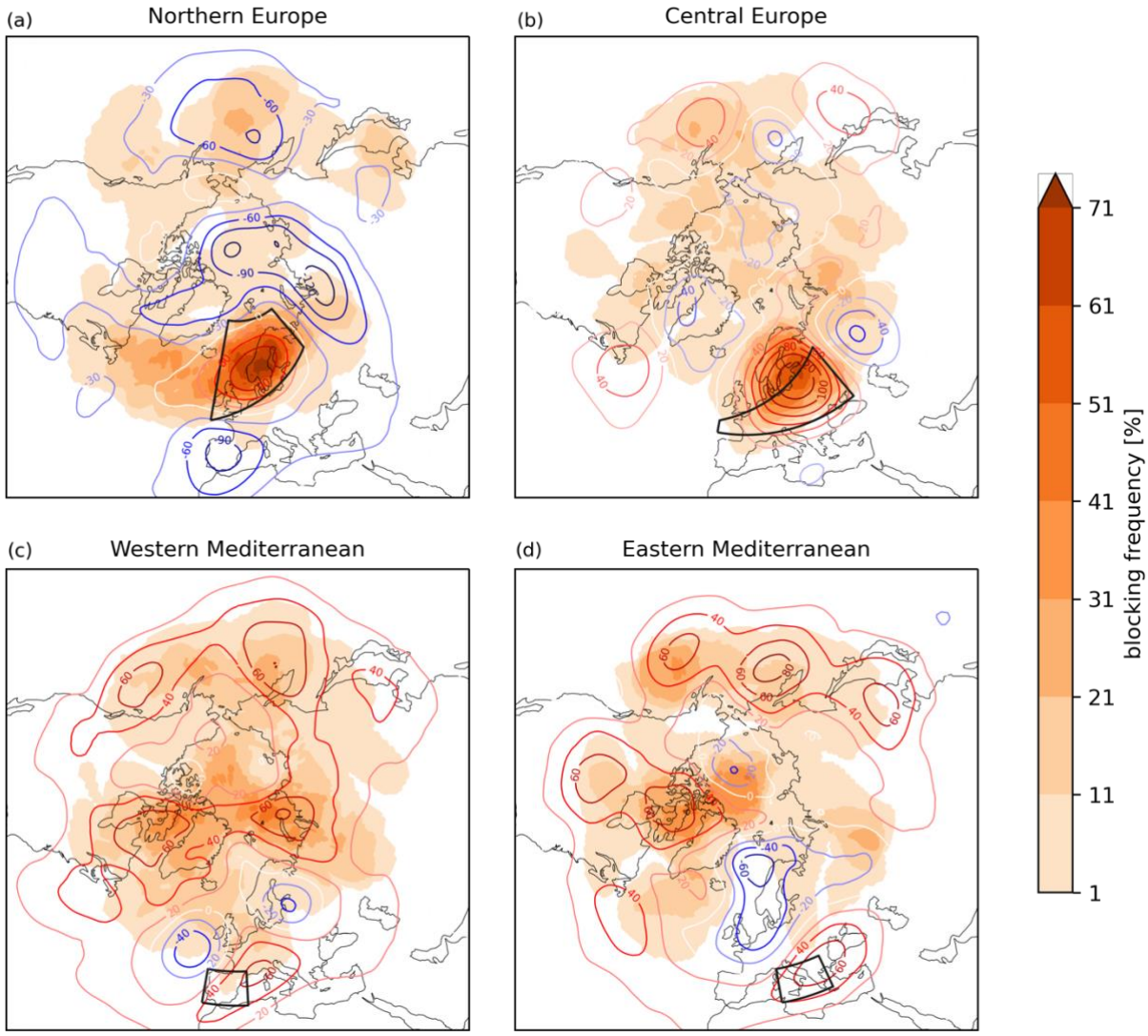

Figure 3.14: Composites of the relative blocking frequency (shaded, in %) and Z500 anomaly (blue contours for negative, red for positive anomalies, in m) during area-weighted mean EFDE of the FWI in summer. The black boxes encompass each study region.

3.4 AVHRR Satellite Data

3.4.1 Active Fire Statistics

Since the fire weather danger indices only depict a potential fire danger, we look at the observed active fire occurrence based on AVHRR satellite data. We select only forest grid points due to the high confidence of the forest class. For this reason, in this section active fires are per definition only forest fires and not wildfires, which also include agricultural fires for example.

Figure 3.15 shows a pronounced north-south divide in Europe in the number of observed active fires per pixel. In Southern Europe, mostly 10 to 50 active fires were detected, on the western Iberian Peninsula it rises above 50 and locally even above 350. The number of observed active fires not only varies regionally but also seasonally (Appendix Figure 6.5). In summer, the number of detected active fires is the highest, followed by a similar amount of observed active fires in spring and autumn. The fewest active fires were detected in winter.

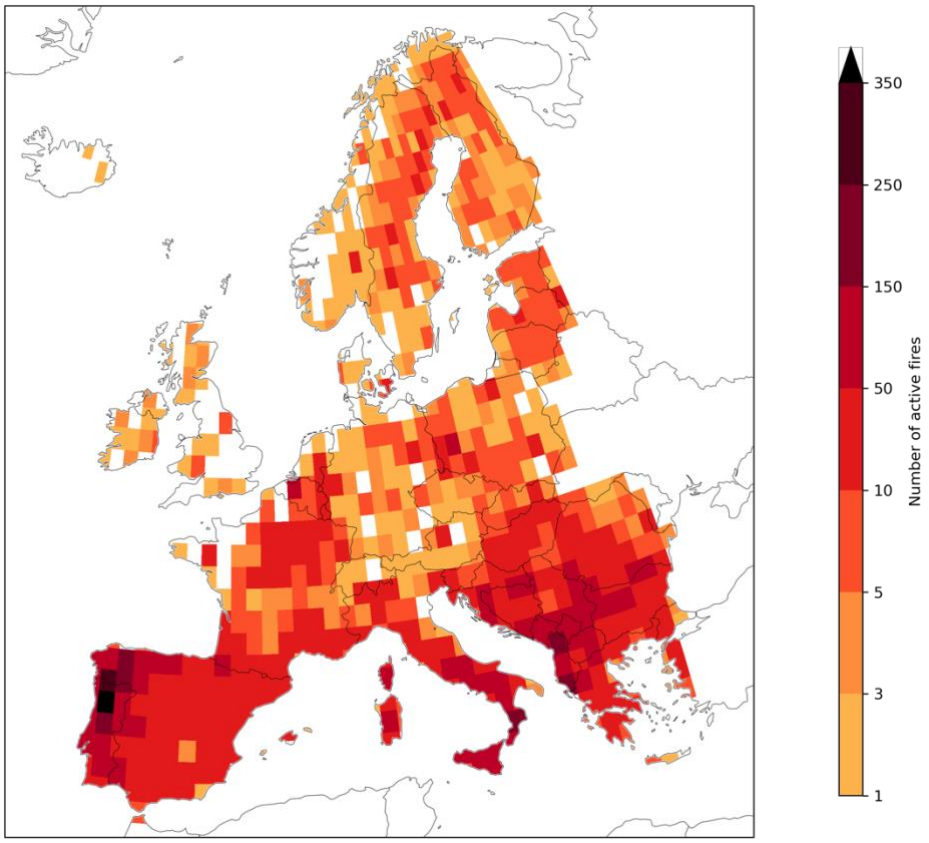

Figure 3.15: Observed number of active fires per grid cell in the period of 1991-2019 in Europe derived from AVHRR satellite data.

The temporal evolution of active fires over Europe reveals a strong temporal variability with peaks occurring mainly in summer and lows in winter (Figure 3.16). The number of monthly observed fires in Europe exhibits a large inter-annual variability.

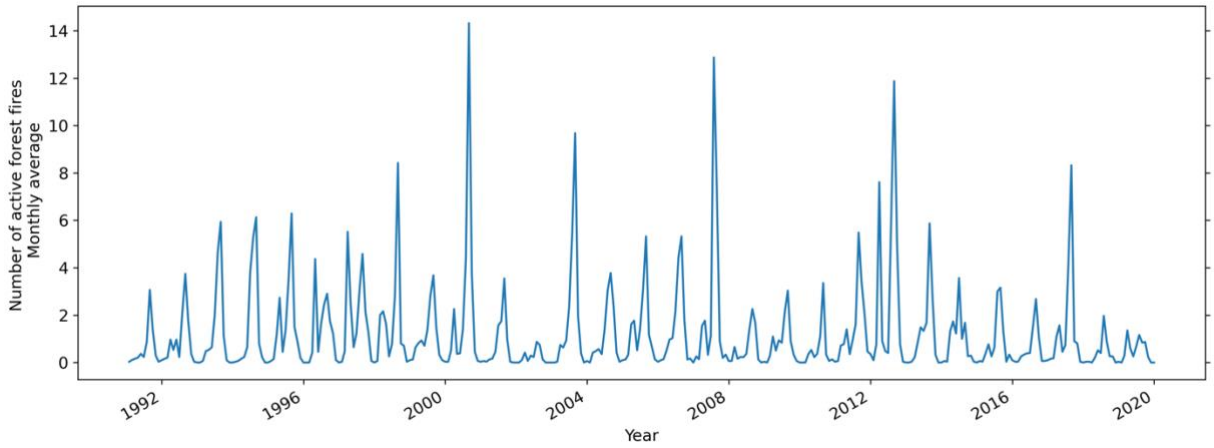

Figure 3.16: Temporal evolution of the monthly mean observed active forest fires from the AVHRR sensor for the period of 1991-2019.

3.4.2 Blocking and Active Fires

Similar to the co-location analysis between blocking and EFDE, we investigate the quality of blocks as an active fire indicator. Figure 3.17 shows the percentages f_{AF} of active fires occurring with a co-located block. We only selected grid points with more than four active fire records per season to avoid random allocations of very low or very high percentages. Thus, all grid cells with less or equal to four active fires in the period of 1991-2019 are masked in white. The spatial pattern is very similar to Figure 3.13 with high f_{AF} in Northern Europe and low f_{AF} in Southern Europe. In Northern Europe, active fires occur in 50%-90% of the cases with a co-located block in summer. In Southern Europe, the relation between blocking and active fires is not very important with f_{AF} values below 20%. Central Europe indicates co-location values between 10% and 50%. Seasonally, only in Northern Europe there is a strong variation with maximum f_{AF} in summer. We also investigate the lagged influence of atmospheric blocking on the occurrence of active fires (not shown). The spatial pattern of lagged f_{AF} does not differ much from Figure 3.17 indicating that the lag has no influence.

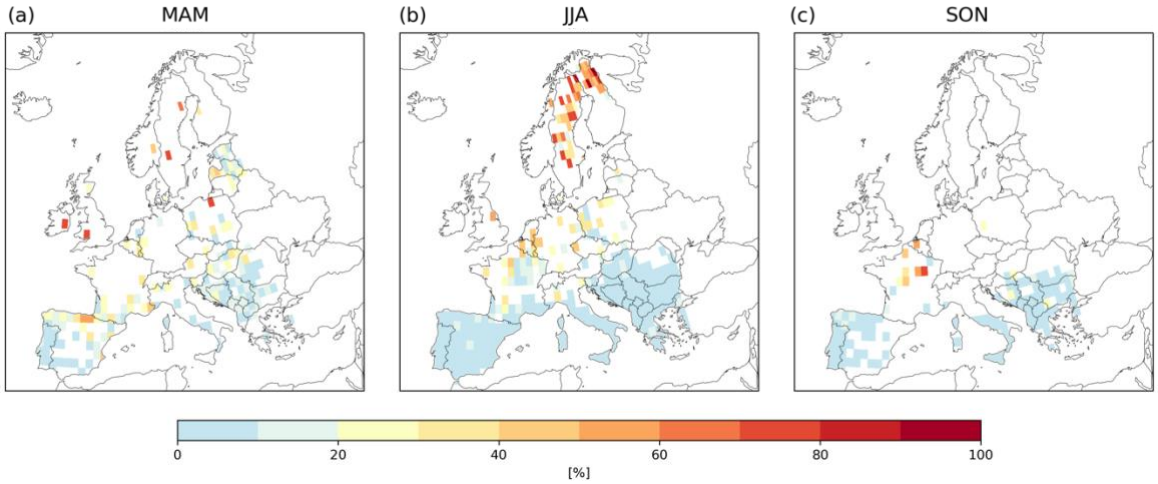

Figure 3.17: Percentage f_{AF} of active fires occurring simultaneously with a blocking event at the same grid cell for (a) spring, (b) summer, and (c) autumn between 1991-2019. Grid points with less than four active fires are masked in white.

3.4.3 Fire Weather Index and Active Fires

In order to validate the ability of the FWI to estimate an active fire correctly, we look at the percentage f_{POD}, which is a metric of how many active fires occurred simultaneously with a FDE in the respective percentile range (>90th, 80th-90th etc.) between 1991 and 2019.

The area-weighted mean f_{POD} over Europe is defined with percentile based on the yearly distribution (Figure 3.18a) and on the seasonal distribution (Figure 3.18b). For both definitions, the f_{POD} increases with increasing percentile range. The ability of the FWI to detect an active fire reaches values of 38-52% for the uppermost percentile range (>P90). This means that about every second active fire is correctly captured by the highest FWI percentile range. The FWI can identify 92% (Figure 3.18a) and 86% (Figure 3.18b) of the observed active fire events when we consider fire weather danger conditions above the median (>P50).

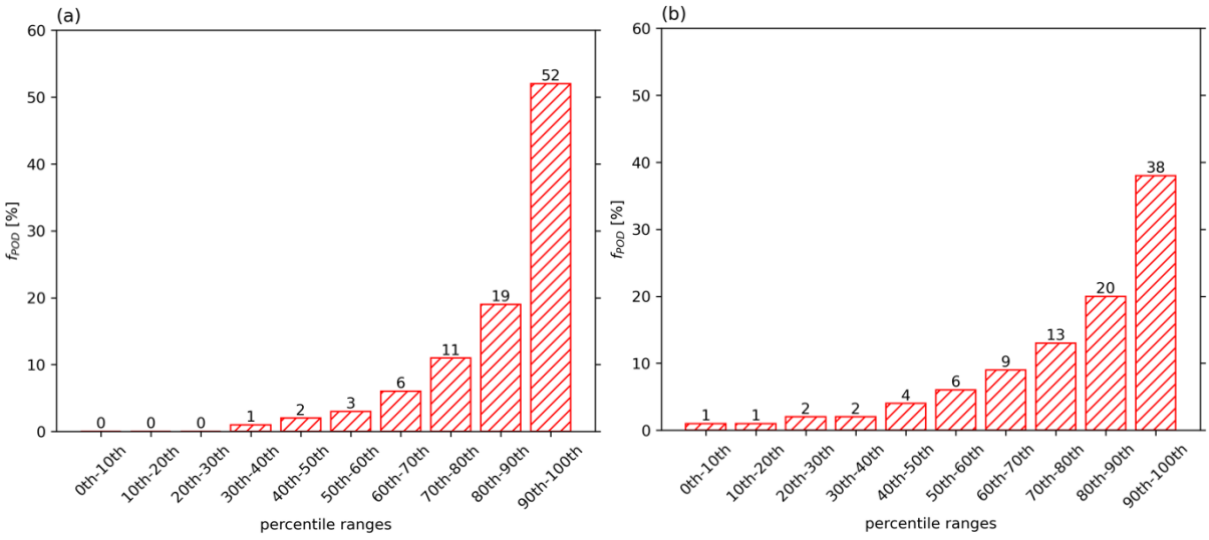

Figure 3.18: The area-weighted mean percentage f_{POD} for the ten percentile ranges based on the (a) yearly and (b) seasonal distribution of the FWI for Europe. (The sum over all percentile ranges does not equal 1 due to the area-weighting.)

From here on we focus on the seasonal percentile definition, since we then deliberately select the same amount of FDE in each season. Figure 3.19 shows the spatial variation of the f_{POD} for >P90. We mask the grid cells with less than four active fires in white. In Southern Europe, the f_{POD} values show a more homogeneous variation than at higher latitudes. The probability to detect active fires is lowest on the Iberian Peninsula with values between 0%-50%. In Southeastern Europe, the f_{POD} is quite high with maximum values between 60% and 80%. In Central Europe and Northern Europe, the f_{POD} is varying a lot more.

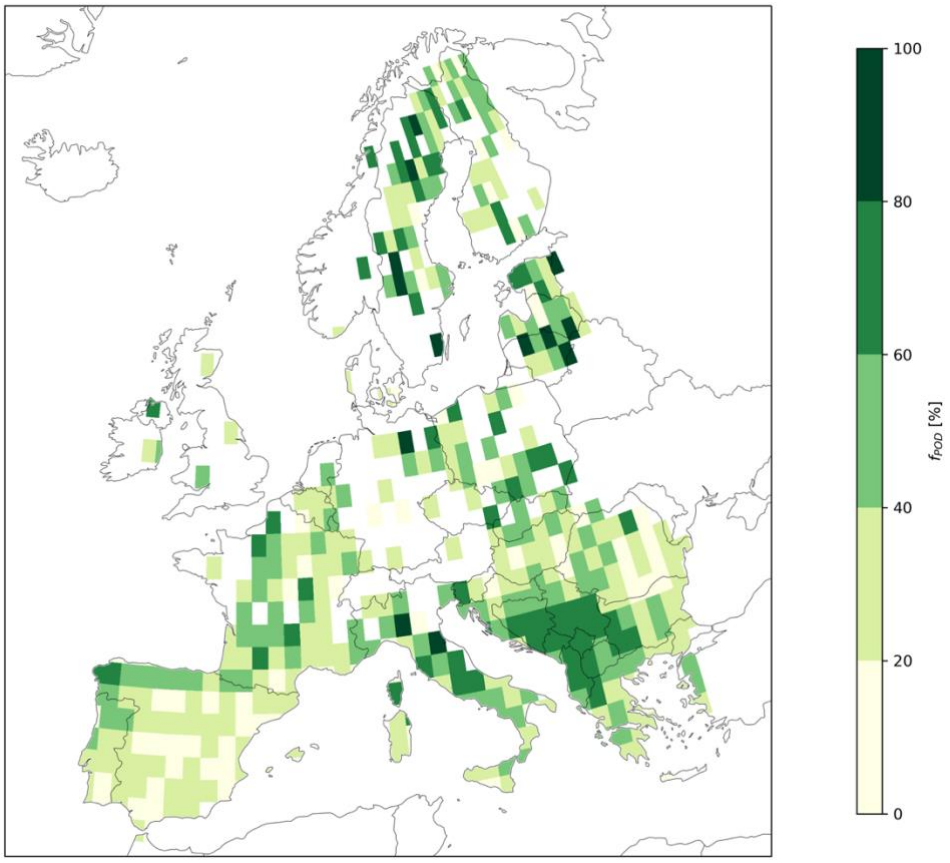

Figure 3.19: Probability of detection f_{POD} for the 90th-100th percentile range for 1991-2019 based on the seasonal percentile distribution of the FWI. Grid points with less than four active fires are masked in white.

In order to assess the ability of the FWI to detect active fires in different regions, we calculate regional averages of the f_{POD} for the four study regions. Figure 3.20, similar to Figure 3.18, shows the highest f_{POD} for >P90 and a decrease with lower percentile range. In Eastern Mediterranean, in 45% of the cases the FWI >P90 is able to estimate an active fire event. This reflects the results shown in Figure 3.20, where the probability of detection is high in Eastern Mediterranean. In Northern Europe and Central Europe, the f_{POD} reaches 40%, while in Western Mediterranean it reaches 27% for >P90. If we consider broader percentile ranges, such as >P70 and >P50, a north-south divide appears in Europe. In Northern Europe and Central Europe, the f_{POD} is higher for the >P70 and >P50 ranges, compared to the Mediterranean regions (Appendix Table 6.1). In Northern Europe, the probability f_{POD} to detect an active fire amounts up to 78% and 92% for >P70 and >P50, respectively. This means that a fire developed in 92% of the time in which the FWI was above the median (>P50) of its climatology between 1991-2019 in Northern Europe.

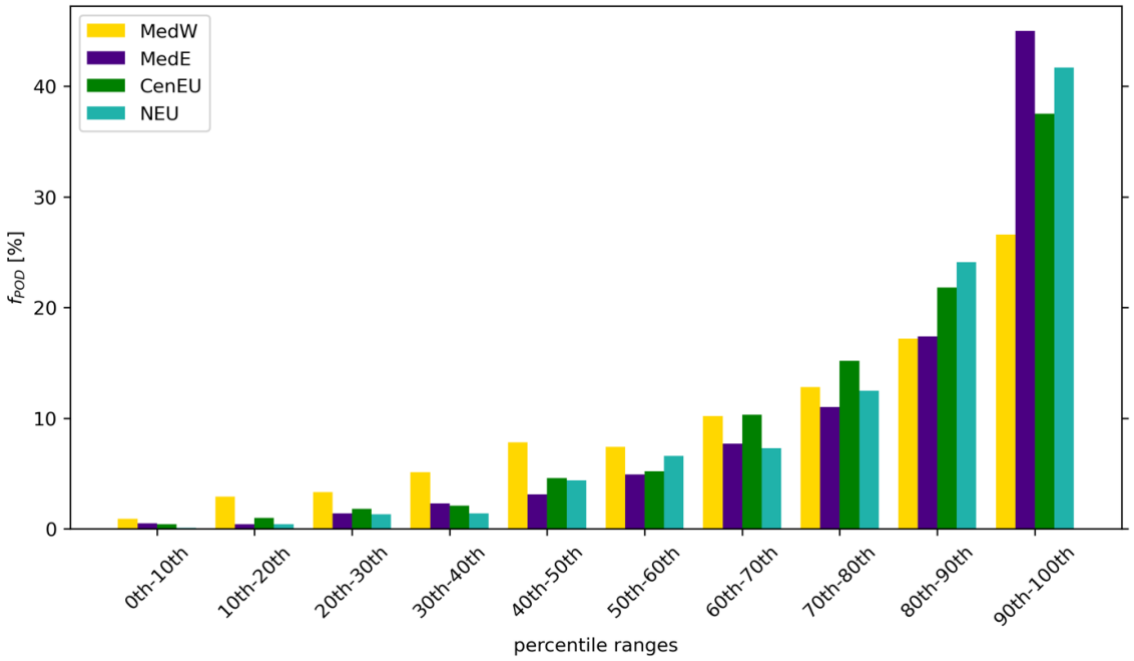

Figure 3.20: Regional area-weighted mean f_{POD} for the four study regions and for ten percentile ranges based on the seasonal distribution of the FWI. Grid points with less than four active fires are masked in white. (The sum does not equal 1 due to the area-weighting.)

We also investigate the seasonal variation of the f_{POD} in Europe (Figure 3.21). In winter, the percentage f_{POD} is highest with 64% followed by autumn with 51% for >P90. Spring and summer exhibit the lowest ability to estimate an active fire correctly. For >P90, spring depicts the lowest f_{POD} values. For the percentile range >P70 and >P50, f_{POD} is lowest in summer with 66% and 82%, respectively (Appendix Table 6.2). A complete overview of seasonal and regional f_{POD} can be found in the Appendix (Table 6.1 and Table 6.2).

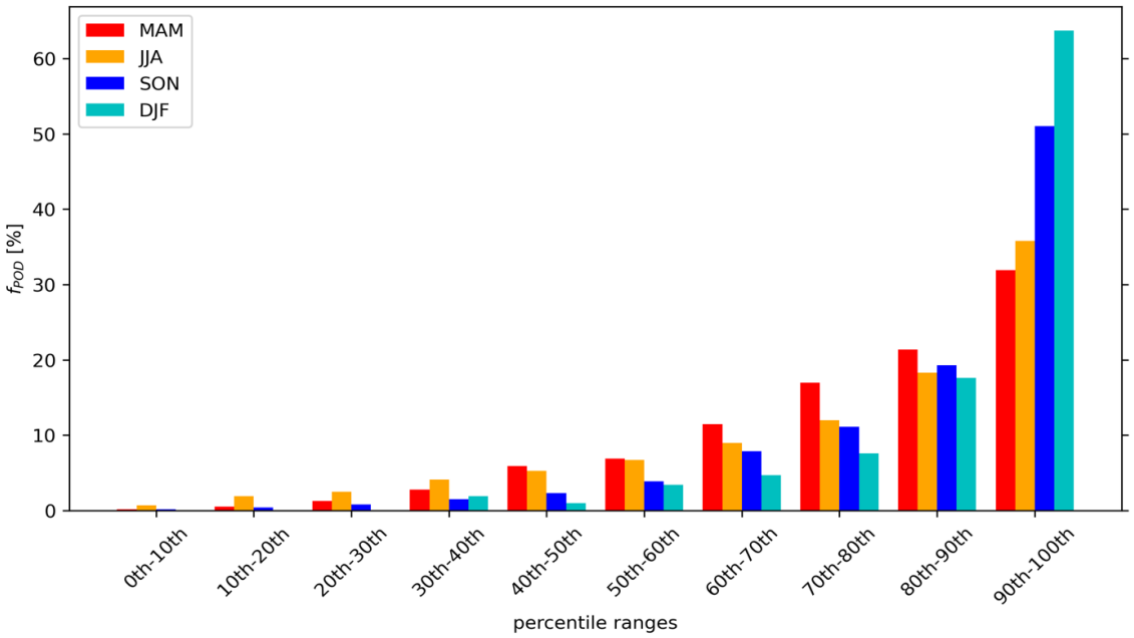

Figure 3.21: Seasonal area-weighted mean f_{POD} for whole Europe and for the ten percentile ranges based on the seasonal distribution of the FWI. Grid points with less than four active fires are masked in white. (The sum does not equal 1 due to the area-weighting.)

3.4.4 BIAS Score

The nature of our approach leads to a systematic overestimation (BIAS > 1) of the occurrence of active fires by the FDE. Figure 3.22 shows the ratio of the number of days in each FWI percentile range (10% of 29 years = ~1060 days) divided by the number of observed fires at each grid cell of Figure 3.15. The BIAS score is same for all percentile ranges, as we look at ten evenly distributed ranges. Since there are not more than 400 active fires observed, the BIAS is always bigger than 1, which corresponds to a systematic overestimation. In regions with more active fires like on the Iberian Peninsula, the BIAS is lower than for example Scandinavia where the frequency BIAS is higher.

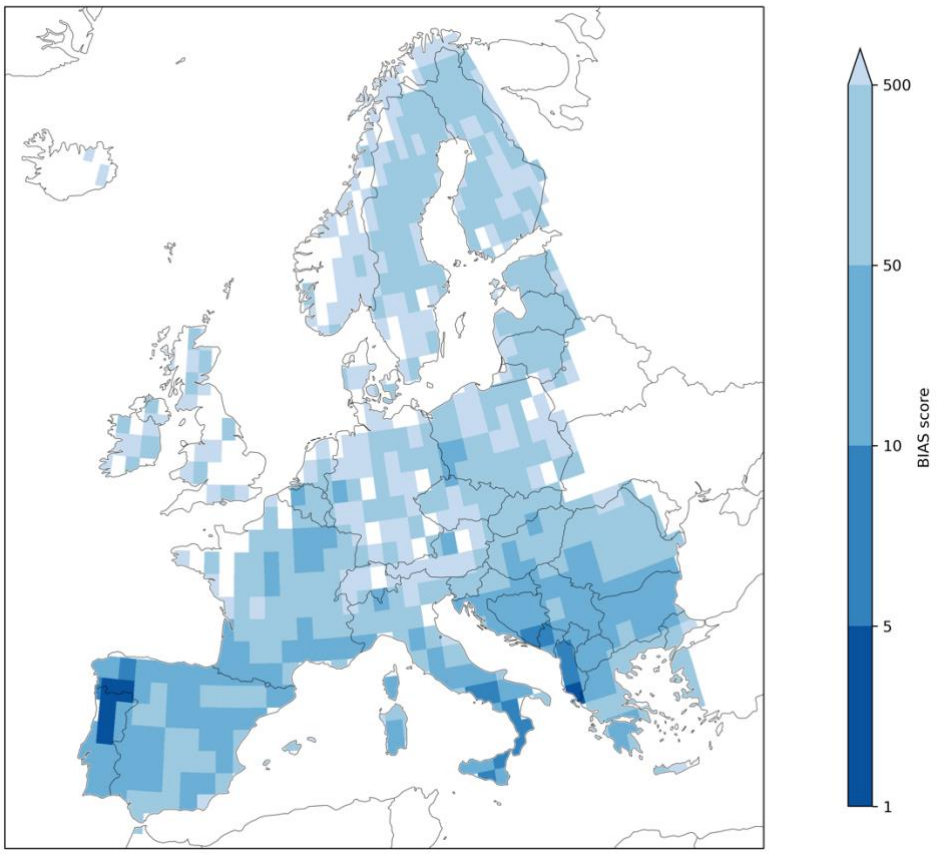

Figure 3.22: Observed number of active fires per grid cell in the period of 1991-2019 in Europe derived from AVHRR satellite data.

4 Discussion

4.1 Case Study Summer 2018

Figure 3.1 shows that the fire weather danger of the summer 2018 varies spatially from month to month, together with the upper-level circulation. High Z500 corresponds to above average fire danger, while low Z500 such as the cut-off low to below average fire danger. When the changes in the monthly Z500 field are high (small), as from July to August (from August to September), the monthly fire weather danger variability is also high (small). The spatial distribution of high fire weather danger depends on the exact location of the block, as do temperature extremes (Kautz et al. 2022). Hence, the case study indicates that Z500 modulates the spatiotemporal variability fire weather danger and thus atmospheric blocking could be a potential driver.

The fuel moisture codes show an anticipated temporal evolution based on their different lagged response time (Figure 3.2a). Of all fire weather indices, four indices (DMC, BUI, ISI and FWI) indicate clear peaks in May and July for Northern Europe in 2018 (Figure 3.2 and Figure 3.3), which co-occur with a Scandinavian blocking. Both May and July correspond to a classical Scandinavian blocking pattern, while June resembles an Atlantic ridge pattern (Grams et al. 2017, Spensberger et al. 2020). Hence, we see that the Scandinavian heatwave of 2018 occurred under a Scandinavian blocking event, which was associated with the unprecedented wildfires in Sweden (Spensberger et al. 2020). The Scandinavian blocking is also clearly visible in the blocking frequencies of May and July (Figure 3.4a). The temperature distribution pattern in 2018 (Appendix Figure 6.1) looks very similar to the blocking frequency pattern in Figure 3.4a, which indicates that blocking drives both the surface temperature and fire weather danger. Especially in summer blocking clearly drives most fire indices but not in winter, the fire danger is low despite high blocking frequencies in November (Figure 3.4b).

If we consider the occurrence of active fires in the summer of 2018, a lot co-occur with above average fire danger (Figure 3.1). However, some regions, such as the Iberian Peninsula, Sicily or parts of the Balkans, display active fires during below average fire weather danger (Figure 3.1b). These regions are highly fire-prone regions, which means that they feature the highest fire occurrence and longest fire period length (Galizia et al. 2022). Even if we have below or near average fire danger in these regions, we still have high temperatures in summer and vegetation that is prone to fire. Especially in the Mediterranean basin, a lot of fires are caused by humans manly due to arson (Ganteaumne et al. 2013). In August 2018, a lot of active fires occurred together with above average fire conditions on the Iberian Peninsula that experienced extremely hot temperatures (Barriopedro et al. 2020). In fact, it was the

hottest Iberian heatwave since 2003 and was driven by an exceptional subtropical ridge, which also appears in the Z500 in Figure 3.1c.

Atmospheric blocking does not only drive the distribution fire weather danger but also the occurrence of active fires, especially in less fire-prone pyroregions like Northern Europe (Figure 3.1b). We conclude that blocks in July 2018 over Northern Europe occurred simultaneously with extreme fire weather danger and the occurrence of active fires. In Southern Europe, above fire weather danger and active fires occurred with a pronounced subtropical ridge. In chapter 4.3, we discuss the relevance of blocking for extreme fire weather danger and the occurrence of active fires quantitatively as well as the capability of the fire weather danger to correctly estimate active fires.

4.2 Descriptive Statistics

The seasonal mean and standard deviation climatologies of the FWI and FFMC show a strong spatial (north-south) and temporal (winter-summer) variability (Figure 3.5-3.8). The little literature available about the fire danger variability over Europe and the connection to the large-scale circulation, emphasizes the importance of this findings. On the other hand, it makes it difficult to compare and contrast the results. For this reason, studies about synoptic weather patterns and other meteorological extremes, such as heat extremes, are considered in order to compare the results.

FWI. In Northern Europe, mean FWI values are low (Figure 3.5) and also the day-to-day variability (spread around the mean value) is low (Figure 3.6). In Southern Europe, the mean FWI and the standard deviation are high. Regions with the largest standard deviations (Southern Europe) are subject to the widest variations in fire weather danger, whereas regions with the lowest values (Northern Europe) have more constant fire weather danger. In winter, the mean FWI values are low with almost no spread, indicating that the fire danger is almost never high. In summer, the variability is larger, which means that the there are days with high fire weather danger and days with low fire danger. The spatial and temporal variability of the seasonal mean FWI climatology (Figure 3.5) correspond to the FWI climatologies of past studies, despite different reference periods (Bedia et al. 2018, Bonk 2019, EEA 2009, EEA 2021).

FFMC. The mean FFMC exhibits a similar spatial and temporal pattern as the FWI with low values in Northern Europe and winter and high values in Southern Europe and summer (Figure 3.7). However, the day-to-day variability of the FFMC is very low in Southern Europe, especially on the Iberian Peninsula. One reason why the Iberian FFMC standard deviation is so low in summer could be due to the rapid response to environmental conditions and the fact that the FFMC stays on a high level if it does not rain. In addition, and more importantly, the FFMC maximum of 99 acts as an upper limit. Since

the mean FFMC is very high and near this maximum on the Iberian Peninsula, the spread around the mean is inherently small. Therefore, the low FFMC variability in Southern Europe occurs because of the narrow distribution near the maximum FFMC value.

Generally, fires begin to ignite at FFMC values around 70, considering the moisture content of the litter (Van Wagner, 1987). If we consider the mean FFMC climatology, is it apparent that on the Iberian Peninsula this threshold is reached in every season and exceeded most clearly in summer (Figure 3.7). This indicates that in Southern Europe, FFMC fire weather danger is so extreme that the occurrence of a fire is only conditional to an ignition source.

Physical Interpretation. To assess the physical meaning of the mean FWI and FFMC fire weather danger and their day-to-day variability across Europe, we compare them with the seasonal climatology of mean average temperature and total precipitation, respectively (Peña-Angulo et al. 2020).

Physically, the strong latitudinal variability of the mean FWI matches the mean temperature climatology between 1979-2017 over Europe with maximum values in Southern Europe, especially on the Iberian Peninsula (Peña-Angulo et al. 2020). The mean FFMC climatology correlates well with total precipitation, which makes sense since it is an index that depends on moisture (Peña-Angulo et al. 2020). The standard deviation patterns of the FWI (FFMC) (Figure 3.6 and 3.8) match well the temperature (precipitation) variability in Europe (Peña-Angulo et al. 2020). The high coefficient of variation (standard deviation/mean) of the mean temperature in Southern Europe confirms the large FWI standard deviation in Figure 3.6. The high variability of the total precipitation in Northern Europe and the Alps corroborates the strong day-to-day variability of the FFMC in Northern Europe and the Alps in Figure 3.8 and the opposite for Southern Europe. Also the seasonal variations correspond well to two the seasonal climatologies of temperature and precipitation from the European Climatology and Trend Atlas of Climate Indices (ECTACI) (Peña-Angulo et al. 2020).

The high FFMC standard deviation in the Alps and in Northern Europe could be due to the low mean, which allows for a greater spread compared to high means as we have seen before. Another reason could be the environmental conditions that change rapidly, influencing the FFMC variability directly.

EFDE thresholds. Figure 3.9 and Figure 3.10 show that the thresholds for EFDE varies across Europe, which means that the definition of EFDE implies very different fire weather danger. In Southern Europe, the FWI fire weather danger is extreme when we define it as an EFDE, but for Northern Europe EFDE occur at low danger levels. Since fire danger maps display the same classes for all countries in Europe, we must be aware of this spatial distinction that most extreme events do not occur in the same danger class for every country. For example, the spring fire weather danger can take on a FWI value as low as

10 in the Scandes and still be an EFDE in a climatological sense for this location. At the same time, the same FWI value in Spain would be far away from an EFDE. Even if one is aware that the fire weather danger is lower at higher latitudes, one still must understand how to correctly interpret fire weather danger maps. Especially for fire action planning it is crucial to evaluate critical fire weather danger situations properly.

This widespread 'Extreme' and 'Very Extreme' danger in Southern Europe demonstrate the importance of the new 'Very Extreme' fire danger class. For the FFMC, we see that particularly in summer, the EFDE thresholds are very high and rarely drops below the 'Moderate' fire danger class. Thus, an additional FFMC similar to the new 'Very Extreme' FWI class could provide remedy for better discrimination. In this thesis, we use EFDE defined based on percentiles, which incorporates the local climatological distribution and is therefore independent on the danger classes.

Pfahl and Wernli (2012a) instigated the relevance of blocking on temperature extremes that can be compared to our results. Temperature extremes are not directly comparable with fire weather danger but as an approximation it constitutes as a comparable data. The geographical distribution of Figure 3.9 and Figure 3.10 looks very similar to the pattern of the 99th percentile maximum temperature (Pfahl and Wernli 2012a). Their results show the highest maximum temperatures in Southern Europe and the lowest in Northern Europe and the Alps, which agrees with our findings.

Seasonality and Temporal Dependence of EFDE. In Figure 3.11, we see that most EFDE occur in summer across Europe. This is consistent with the mean FWI climatology (Figure 3.5), which also shows the highest values in summer. The second highest occurrence of EFDE reveals a north-south divide, which shows that in Southern Europe there are more EFDE in autumn and in Northern Europe more in spring (Figure 3.11b). The only deviations are in the Alps and in Scotland, where the EFDE are not clearly assigned to one season maybe due to the fact that the we have a lot of rain throughout the year with high variations locally. Figure 3.12 reveals that EFDE are more persistent events in Central and Northern Europe, while in Southern Europe, especially on the Iberian Peninsula, EFDE manifest themselves as more isolated events with low temporal dependence. The high temporal dependence in Northern Europe suggests that persistent meteorological conditions, such as atmospheric blocking, could be a potential driver for high fire weather danger. Thus, in the following subsection 4.3 we discuss the f_{EFDE} of Figure 3.13, which quantifies the relevance of atmospheric blocking for simultaneous EFDE.

Seasonal blocking frequency. Lastly, we discuss the seasonal blocking frequencies shown in Figure 2.3. Europe is a region with high blocking frequencies due to the location of the North Atlantic storm track, which is meridionally tilted upstream of Europe (Kautz et al. 2022). Due to the definition of the blocking index, blocks occur more often at higher latitudes (Figure 2.3). Most blocks appear in

Scandinavia and over Western Russia, which are called Scandinavian blocking and Ural blocking (Grams et al. 2017, Spensberger et al. 2020). The spatial pattern of atmospheric blocking resembles the results from previous studies (Pfahl and Wernli 2012a, Pfahl 2014, Schwierz et al. 2004, Sillmann and Croci-Maspoli 2009). However, some blocking climatologies indicate maxima more over the North Atlantic than over Northern Europe and also the magnitude of the blocking frequency differs. Since the definition of the blocking index defines the position of a blocking system, another blocking index definition could lead to different results (Kautz et al. 2022). For example, our modified blocking index, that is based on Z500 anomalies shows more blocks at lower latitudes, while their index based on PV do not capture low latitude blocks very well (Pfahl and Wernli 2012a).

4.3 Blocking and Fire Weather Indices

Figure 3.13 shows that the FFMC reaches higher f_{EFDE} values (d-f) than the FWI (a-c). The reason behind that could be that the FFMC is characterized by rapid changes and thus a faster reaction to environmental conditions. Since the environmental conditions are influenced by clear-sky conditions and subsidence associated with the block, the FFMC reacts more rapidly and thus exhibits higher f_{EFDE}. According to Pfahl and Wernli (2012a), in all regions where f_{EFDE} is many times greater than the climatological blocking frequency, there is a statistically highly significant relationship.

There are regional and seasonal differences of the f_{EFDE}, with highest f_{EFDE} in Northern Europe and in summer (Figure 3.13). Since most blocks are located over Northern Europe, it makes sense that also the highest f_{EFDE} occur there. In Northern Europe, the highest f_{EFDE} in summer does not correspond to the seasonal blocking frequencies, which are highest in autumn (Figure 2.3). This suggest that the relevance of blocking for EFDE is very high in summer in Northern Europe, but also statistically significant in the other seasons. In the Mediterranean, the highest f_{EFDE} in the Mediterranean occur in spring, corresponds to the seasonal blocking frequency that is highest in that season (Figure 2.3). However, the f_{EFDE} in the Mediterranean is still low, which means that blocks are irrelevant for EFDE at the same location. The f_{EFDE} for P95 and P97 show the same spatial pattern but with lower co-location values indicating that blocking is very relevant for the most extreme fire danger events (Appendix Figure 6.2 and Figure 6.3)

The results from the lag analysis for the FWI suggest that in summer the EFDE are more dependent of the accumulated blocking influence of the last week (not shown). In spring and autumn, the single active block seems to be of more importance than the blocking conditions of the last week. This could be an indicator that the feedback of atmosphere and soil moisture plays a more important role in summer, which would have to be investigated further. For the FFMC, the lag does not play a significant role in all seasons. Since the FFMC describes the fuel of the litter layer that reacts very rapidly to changing environmental conditions, it is more dependent on the present-day weather conditions than on the past.

On the other hand, the FWI incorporates the information of indices (DC and DMC) that accumulate the moisture conditions and thus the weather of the previous weeks.

As a matter of fact, there is little literature available that quantifies the relevance of atmospheric blocking for co-located EFDE. On the one hand, this emphasizes how novel the findings of this thesis are, but, on the other hand, makes it difficult to compare and contrast the results. For this reason, studies about blocking and other meteorological extremes, such as heat extremes, are considered in order to compare the results of this thesis.

The co-location results in chapter 3.3 indicate that a substantial portion of EFDE over mid to high latitudes occur simultaneously with atmospheric blocking at the same location. The spatial pattern of f_{EFDE} in Figure 3.13 shows a high co-location in Northern and Western Europe and low co-location in Southern Europe, which corresponds to the results of co-located temperature extremes and blocking over Europe (Brunner et al. 2018, Pfahl and Wernli 2012a, Stefanon et al. 2012). They found that the highest co-location of warm temperature extremes and blocks occur in summer, which coincides with our result (Figure 3.13 and Table 3.1). There are some deviations, for example in France and Spain, where other studies show the co-location of blocking and temperature extremes not to be significant (Pfahl and Wernli 2012a). As mentioned before, this may be due to the blocking index for which we use of Z500 anomalies from ERA5, while Pfahl and Wernli (2012a) use PV anomalies from ERA-Interim.

Regions with high f_{EFDE} are associated to typical blocked weather regimes such as the Scandinavian blocking for Northern Europe, the Atlantic ridge for Great Britain or the Ural blocking in Western Russia (Grams et al. 2017, Spensberger et al. 2020). The two weather regimes Scandinavian blocking and Atlantic ridge did also play an important role in the extremely hot summer of 2018 (Chapter 3.1). To investigate that in more detail, one could include weather regimes to analyze the occurrence of EFDE throughout different regions in Europe.

Zschenderlein et al. (2019) suggested that warm-air advection from warm regions is of minor importance for heatwaves in Scandinavia compared to *in-situ* warming in the center of the block. If we assume that heatwave conditions are comparable with conditions leading to fire prone conditions, we can say that the high f_{EFDE} found over Scandinavia (Figure 3.13) agree with their findings. In general, previous studies found that atmospheric blocking induces warm surface conditions through subsidence and diabatic heating in the central part of the block (Spensberger et al. 2020, Zschenderlein et al. 2019). Enhanced solar radiation due to below average cloud cover associated with blocking leads to amplified surface evaporation. Together with the negative precipitation anomaly the land surface desiccates leading to larger sensible heat fluxes and to an intensified build-up of heat (Miralles et al. 2014, Pfahl and Wernli 2012a). These dry conditions exacerbate the fire danger below the center of the block, which

often lies over Northern Europe. Potential far-field effects of the anticyclonic circulation are not considered in this co-location analysis but will be discussed in the next chapter where we conduct a regional analysis of EFDE.

4.3.1 Regional Analysis

In Figure 3.14, we show that in Northern and Central Europe EFDE co-occur with blocking but not in Southern Europe similar to the results of Figure 3.13. On the other hand, all four regions exhibit positive Z500 anomalies during EFDE, which corroborates previous studies that investigated the relationship between temperature extremes and upper-level ridges or blocks (Pfahl and Wernli 2012a, Sousa et al. 2018, Zschenderlein et al. 2019).

The fact that blocks do not occur simultaneously with EFDE in Southern Europe is consistent with past studies (Sousa et al. 2018, Spensberger et al. 2020, Stefanon et al. 2012). In addition, Zschenderlein et al. (2019) found that heatwaves over Scandinavia are associated with blocks while they are accompanied by subtropical ridges over the Mediterranean. This highlights the importance of differentiating between high-latitude blocking and subtropical ridges as they have different impacts on different regions (Sousa et al. 2018, Zschenderlein et al. 2019). Therefore, in the following we will discuss the prevalent large-scale circulation during EFDE for every region separately.

Northern Europe. High blocking frequencies and overlapping positive Z500 anomalies indicate a great relevance of atmospheric blocking for EFDE in Northern Europe (Figure 3.14a). The persistent and quasi-stationary anticyclonic circulation disrupts the normal westerly flow at mid-latitudes and leads to several extreme weather events in and around the block (Kautz et al. 2022). The surface cyclones are being redirected around the block, which can be seen by the negative Z500 anomalies north and south of the block (Figure 3.14a) (Kautz et al 2022). Over the Iberian Peninsula, there appears a negative upper-level anomaly that leads to rather low fire weather danger there. This is similar to the findings of Sousa et al. (2018), that show blocking anticyclones over Northern Europe to be associated with below average temperatures at lower latitudes due to the southward shifting of the low-pressure systems. Hence, we can say that, on the one hand, atmospheric blocking is of major importance for EFDE in Northern Europe. On the other hand, blocking seems not to be a dynamical driver for EFDE in Southern Europe, regardless of the location of the block.

Central Europe. In Central Europe, atmospheric blocking is also an important feature for EFDE in this region, which agrees with the results of previous studies (Figure 3.14). The Central European is not always defined identically to the one we used but should still be comparable. Bieli et al. (2015) explained in their work that three days prior the onset of a heatwave, most air parcels are already located over

Central Europe, which suggests the influence of a persistent weather pattern such as blocking. To understand heatwaves, Zschenderlein et al. (2019) investigated the residence time of the air parcels over the respective target region (circles with 500 km radius) by calculating forward trajectories and determining when the trajectories exited the region. Their assumption is that the longer the air parcels reside over the area of interest, the more important become potential feedbacks mechanism of the atmosphere and the land surface. The longest residence time is found for Scandinavia and Central Europe where the air parcels stall around 1.5 days in the target region (Zschenderlein et al. 2019). The authors state, that it is possible that the air parcels could be exiting and re-entering the target region again, which presumably occurs jointly with a blocking event. Thus, the air masses leading to hot temperature extremes at the surface are not stationary even though the synoptic blocking anticyclone is quasi-stationary. Instead, new air masses that undergo warming by subsidence and diabatic heating near the surface replace the old air masses (Zschenderlein et al. 2019). Also Bieli et al. (2015) described the importance of the local soil conditions on diabatic heating and *in-situ* warming, which are very often associated with atmospheric blocking. These similarities indicate that the processes leading to heatwaves occurring with simultaneous blocking events are also responsible for EFDE in Central Europe.

Western Mediterranean. In Southern Europe, Figure 3.14c and d show that blocks are not of relevance for EFDE but rather narrow ridges visible as positive Z500 anomalies. Previous studies indicated for the Iberian Peninsula, that shortly before the onset of a heatwave, air parcels typically ascend after a prolonged period of subsidence (Bieli et al. 2015, Santos et al. 2015, Zschenderlein et al. 2019). This could be due to heating near the ground and the subsequent formation of a heat low (Santos et al. 2015). In Figure 3.14c, the upper-level geopotential anomalies show that the Iberian Peninsula lies west of the ridge axis, between the ridge and the upstream trough. There, the effect of subsidence is not as substantial as in the ridge axis, which enables the formation of a surface heat low. Additionally, from atmospheric dynamics theory, we expect to have rising motion where we have divergence of the ageostrophic flow, which is located downstream of a trough. In our case, this would foster the formation of a thermal low over the Iberian Peninsula, which induces convergence of air masses towards the inner peninsula (Santos et al. 2015). This, in turn, leads to strong diabatic warming by surface fluxes due to the long residence time of the air parcels over land. Thus, the mechanism of a heat low seems not only to be an important mechanism for temperature extremes but also for the occurrence of EFDE over the Western Mediterranean. Indeed, Hoinka et al. (2009) showed that the Iberian heat low occurs three days before the peak amount of burnt area. During these days, the thermal low transports heated air towards the western Iberian Peninsula and Portugal. In addition, strong heat lows at lower latitudes could even be the reason for the non-existent relationship between blocking and EFDE similar as for temperature extremes (Pfahl and Wernli 2012a).

The north-east displacement of the upper-level ridge axis leads to the formation of a surface anticyclone beneath, with centre near Switzerland and Austria. Thus, the surface air masses would be transported towards the Iberian Peninsula from easterly directions. Previous studies corroborate this, by showing that warm continental air masses, transported mostly by easterly or southeasterly flow directions, are responsible for heat extremes over Spain and Portugal rather than southerly winds from North Africa (Pfahl 2014, Santos et al. 2015).

Eastern Mediterranean. Figure 3.14d indicates positive Z500 anomalies of a subtropical ridge with maximum on the northeastern edge of the box encompassing Eastern Mediterranean. Pfahl (2014) corroborates this result as he finds positive blocking anomalies northeast of the target region and emphasizes the role of easterly horizontal advection of warm air for hot temperature extremes. The air parcels that lead to heatwaves in the Eastern Mediterranean descend rapidly before entering the planetary boundary layer (Zschenderlein et al. 2019). Thus, on the one hand we have strong subsidence that causes strong adiabatic warming and on the other hand we also have diabatic warming. The latter occurs not long before the heatwave onset, since the increased solar radiation leads to enhanced surface sensible heat fluxes. For Eastern Mediterranean, remote surface conditions have been shown to be important for temperature extremes, but not through advection of warm air (Zschenderlein et al. 2019). Rather, the transport above remote dry soils and associated surface fluxes strongly impacts the local temperature extremes, which is called “event self-propagation” (Miralles et al. 2019, Zschenderlein et al. 2019). Therefore, we notice that past studies are not in agreement on the role of warm air advection for temperature extremes, however, they do agree that air parcels, which are responsible for heatwaves in the Eastern Mediterranean are partly due to remote surface conditions and the heat transfer due to sensible heat fluxes. Assuming that heatwaves and fire danger are similar in their development, these processes could be also of importance for EFDE in Eastern Mediterranean.

Previous studies showed that heatwaves in Southern Europe occur while there is a zonal weather regime present over the rest of Europe (Zschenderlein et al. 2019). This corresponds to the mean Z500 circulation during EFDE in Southern Europe (Appendix Figure 6.4). The upper-level flow configuration for both Mediterranean regions imply a rather dynamic weather pattern with a pronounced trough upstream that modulates the downstream changes of the weather pattern. For this reason, flat ridges over the Mediterranean region seem to have a rather short lifetime compared to persistent atmospheric blocking over Northern Europe. That corroborates the fact that persistent blocking events in Northern Europe lead to temporal dependent EFDE while on the Iberian Peninsula and Eastern Mediterranean subtropical ridges lead to more isolated EFDE (Figure 3.12).

At this point, we have to discuss some limitations to our regional analysis approach. First of all, as we make composites over several time steps and for an area-weighted mean of EFDE, it is difficult to detect

one clear synoptic pattern that can be made responsible for all EFDE in the whole region. Hence, it makes it also difficult to screen out the dominant dynamical mechanism that drives forest fire danger. Sousa et al. (2018) mentioned that summer temperature extremes over southern Europe are highly dependent on the exact location of the sub-tropical ridge. Thus, it is difficult to find a full explanation for a region with a composite of the upper-level geopotential height pattern. Fire occurrences vary substantially across different regions as shown for Mediterranean France or also continental Spain (Rasilla et al. 2010, Ruffault et al. 2017). In that sense, an analysis on a smaller spatial scale would be required to address local extreme events and the connection to local weather pattern.

4.4 AVHRR Satellite Data

4.4.1 Active Fire Statistics

The spatial and temporal variability of the observed active fires between 1991-2019 (Figure 3.15) is very similar to the mean climatologies of the fire weather danger indices (Figure 3.5 and 3.7) and the variability of EFDE (Figures 3.10-3.12). The mean FFMC climatology (Figure 3.7) shows that in Southern Europe, the fire danger is so high that the occurrence of a fire only depends on an ignition, which corresponds to the high number of active fires in the Mediterranean (Figure 3.15). In Southern Europe, a lot more active fires were observed compared to Northern Europe corresponding to the temperature and precipitation climatologies discussed before. With locally over 350 active fires, Portugal is the most affected country according to the active fires detected by the AVHRR sensor. The spatial pattern resembles the number of active fire days of the Global Fire Emissions Database (GFED4) dataset between 2000 and 2013 (Di Giuseppe et al. 2016).

The temporal evolution of the monthly averaged active forest fires (Figure 3.16) captures some of the most extreme fire seasons such as the summers of 2003, 2007 and 2012 (De Rigo et al. 2017). The timeseries corresponds to the temporal evolution of the number of forest fires between the period 1985-2019 that is divided into different types of forests (Weber 2021).

4.4.2 Blocking and Active Fires

The co-location of active fires occurring simultaneously with a block at the same grid point reveals very similar results as for the EFDE (Chapter 3.3). In Northern Europe, where we have more than four active fires between 1991-2019, at least every second active fire occurs with a co-located block. Even though the occurrence of active fires is very variable, the result indicates a strong relevance of blocking for the active fire occurrence in Sweden mainly. In Southern Europe, we have a lot more active fires (Figure 3.15) and thus the result shows a smoother variation but blocking is not a good indicator there. Even

though active fires are mainly dependent on the ignition of the fire rather than on the predominant weather pattern, we see that most active fires in Northern Europe occur together with atmospheric blocking. The lower co-location with a lag could be due to the fact that active fires depend mainly on the ignition. On the other side, the occurrence of active fires is random and thus partly independent of past weather conditions.

Past studies investigated only small regions about the influence of different weather patterns on the occurrence of fires and are mainly restricted to Southern Europe where most fires occur. Ruffault et al. (2017) found that large fires in Mediterranean France do not occur with blocking but rather during the Atlantic ridge weather regime. Another study for continental Spain showed that the magnitude of fire danger conditions varies substantially across different regions and correlate with different weather patterns such as enhanced Z500 (Rasilla et al. 2010).

4.4.3 Fire Weather Indices and Active Fires

As forest fire danger quantifies only a potential danger, in a next step we incorporate satellite data with the active fire occurrence in order to validate the fire danger indices. The so-called potential predictability, the evaluation of the achievable skill of the FWI component, is determined by comparing reanalysis fire weather indices with the observed active fires occurrence.

For the seasonal and yearly definition respectively, 38% and 50% of all observed active fires across Europe occur during high FWI fire danger (>P90). In general, the probability of detection f_{POD} based on the yearly FWI distribution is higher than for the seasonal FWI distribution (Figure 3.18a and b). The reason is that with the yearly definition we select much more fire danger days in summer compared to the other seasons since then the fire danger is highest, creating a summer bias. Since we have most active fires occurring in summer (Appendix Figure 6.5), the probability to have matches with active fires is higher compared to when we consider each season separately. To illustrate this summer bias, an example for the year 2017 reveals that all >P90 fire danger days occur in summer, which leads different matches than if we define >P90 for every season separately (not shown).

The seasonal f_{POD} is lowest in summer and highest in winter as we have seen in Figure 3.21. The reason is that in summer we have a lot of active fires, mostly on the Iberian Peninsula, where the probability of detection is very low (Figure 3.20). Thus, also the summer f_{POD} is low. In winter, we have much fewer active fires occurring in Central Europe rather than in Southern Europe (not shown). This results in a higher ability to detect active fires as Central Europe shows a higher f_{POD} (Figure 3.20). In addition, in winter we have low FWI values most of the time (Figure 3.5) and it seems that FWI is high when an

active fire occurred. In contrast, in summer there are a lot of days with high fire danger, which leads to a lower hit rate.

Optimally, the FWI would be able to discriminate between fire occurrence and non-events (Di Giuseppe et al. 2016). This would mean that it indicates high fire danger when an active fire was observed. In Figure 3.18, 3.20 and 3.21 this would correspond to a left-skewed distribution and in case of a perfect estimation of just one distinct spike in the highest percentile range (>P90). All three Figures indicate that the f_{POD} to decreases with lower percentile ranges, which is desirable as it indicates a high potential predictability of the FWI. The area-weighted f_{POD} for whole Europe, for each study region and for each season (Figure 3.18, 3.20 and 3.21) shows that the highest FWI percentile range (>P90) is best in detecting active fires. Thus, most active fires do not occur during moderate fire danger, when people maybe are less attentive and sensitized compared to during extreme fire danger conditions, as one might assume. Instead, the highest percentile range also achieves the highest probability of active fire detection.

In order to compare our findings, we summarize the relevant results of this thesis with past literature (Table 4.1). Di Giuseppe et al. (2016) and Di Giuseppe et al. (2020) assess the FWI and its capability to detect fire on a global scale. We compare our results with their findings for Europe. Di Giuseppe et al. (2016) used ERA-Interim reanalysis data for the FWI and 11 years of observed burned areas from the Global Fire Emissions Database (GFED4). Di Giuseppe et al. (2020), on the other hand, used ECMWF high-resolution forecasts (HRES) to calculate FWI and daily maps of Fire Radiative Power (FRP) from the Global Fire Assimilation System (GFAS) using observation of the MODIS for the year 2017. Thus, we see that the datasets and the study period differ but still we can compare the results. Both past studies use the yearly distribution of the FWI to calculate the percentiles, as they performed a global analysis and summer occurs at different times of the year depending on the latitude.

Our results show that in 86% and 92% of the cases, depending on the seasonally or yearly definition, the FWI above the 50th percentile (>P50) is able to detect an active fire (Table 4.1). Di Giuseppe et al. (2016) found a very similar percentage of 86% for the FWI. For >P75 their result of 60% is lower compared to the 64% and 78%. Di Giuseppe et al. (2020) studied the year 2017 only, which is why we also calculated for that year alone. They used ECMWF HRES forecasts with lead times of 1 to 10 days. The f_{POD} for all years (2017 only) is 38% and 52% (34% and 46%) compared to their results of 50%-59% depending on the lead times for Europe (Di Giuseppe et al. 2020). The percentages for 2017 are lower compared to their findings and for years we receive similar results (38% and 52%). Another study assessed the probability of detection using FWI from ERA-Interim and GFED4 burned area from MODIS between 2003 and 2015 (Vitolo et al. 2018). They define FWI EFDE not on percentiles but for FWI > 21.3, which makes it not directly comparable with our results. However, if we assume this FWI

threshold definition to be similar to >P90, their result of 47% probability to detect burned area is among the range of our results.

The regional pattern of the probability of detection (Figure 3.19 and Figure 3.20) differs from previous findings. Generally, the highest values were observed in the Mediterranean and in boreal forests compared to lower values in Central Europe (Di Giuseppe et al. 2016, Di Giuseppe et al. 2020). They argued that the FWI performs better in regions where the fire regime is moisture limited (Mediterranean and boreal forests) compared to regions where it is fuel limited (Central Europe). Abatzoglou et al. (2018) investigated the correlation between burned area and the seasonal FWI and shows a quite strong relationship in Northern Europe and Eastern Mediterranean. Our results suggest that the probability of detection is highest in Northern Europe for >P50 and >P70 corresponding to their results. For >P90, however, Easter Mediterranean attains the highest f_{POD} values. Central Europe, on the other hand exhibits higher f_{POD} values than the Mediterranean for >P50 and >P70. We see that depending on the percentile ranges considered, the capability of the region changes. The fact that Eastern Mediterranean has the highest f_{POD} indicates that there the system is performing best for FDE >P90, which correspond to past studies. If we look at the FWI performance for fire danger above the median (>P50) for example, Northern Europe exhibits the highest f_{POD}. Yet, if we consider the potential of the highest FDE estimates >P90, then Eastern Mediterranean is the region where most active fires were accurately detected. Therefore, Eastern Mediterranean seems to be the best region for the FWI to detect active fires during EFDE and in Northern Europe depicts the highest probability to detect active fires for above average FWI fire danger conditions.

The deviations could stem from the fact that we only incorporate forest fires, while previous studies also look at agricultural fires or fires on shrublands or grasslands (Di Giuseppe et al. 2016, Di Giuseppe et al. 2020). Another reason could be that some past studies use different metrics such as the extremal dependency index (EDI) to assess the potential predictability (Di Giuseppe et al. 2016).

In sum, our thesis provides very similar FWI verification results as past studies presented. However, despite similar results, there are some deviations, which can be due to different factors. In the next section, we discuss different reasons and limitations that could explain the discrepancies.

*Table 4.1: The area-weighted mean f_{POD} for several percentile ranges (>P50, >P70, and >P90) based on results of this thesis and from past literature. (*depending on lead times of the forecasts).*

		>P50	>P75	>P90 (2017)
Results	Yearly percentile	92%	78%	52% (46%)
	Seasonal percentile	86%	64%	38% (34%)
Literature	Di Giuseppe et al. 2016	86%	60%	–
	Di Giuseppe et al. 2020	–	–	(50%-59%)*

First of all, we discuss the limitations of the AVHRR active fire data used in this thesis. The AVHRR sensor was not constructed for fire detection, which indicates that it is not a perfect fire detection measurement device. The extraction of active fires is limited by the viewing geometries of the satellites and by the position of the sun that can cause sun glints (Weber and Wunderle, 2019). In addition, the detection capability of the AVHRR sensor is limited by the low saturation temperature of the MIR channel and thus capped by the maximum temperature it can register (Weber and Wunderle, 2019). Therefore, very large and hot fires are missed and also the smallest and coolest fires, as they do not elevate the MIR channel response sufficiently to be distinguished from the noise in the surface and atmosphere (Giglio et al. 1999). Further limitations include that the satellite must pass over the active fire region in order to detect it. Clouds also pose a problem to detect potential active fires. In Scandinavia, the vast number of lakes pose a big challenge, since even a slight shift in the water body mask can lead to an erroneous detection of an active fire due to sun glint. Despite the integrated filter that screens for sun glints and other potential sources of errors, some cases could be missed, which is why the detected fires have to be treated with caution. For this reason, we only selected pixels with more than four active fires so that random matches do not get a great weighting. Lastly, orbital drifting effects of satellites can influence the temperature of fire pixels on an interannual scale, which can significantly reduce the number of observed fires (Weber and Wunderle, 2019). For this thesis, we assume that the AVHRR sensor correctly identifies active fires, but we cannot know for sure how many it falsely detected and how many it misses. However, since we only use the forest fires with the highest confidence estimate, we expect this bias to be small. Despite these inherent limitations of the AVHRR sensor, other potential factors contribute to deviations from previous studies, which are discussed in the following.

In Chapter 2.2.5, we described that in this thesis we investigate retrospective estimations of fire weather danger and not forecasted data. Prior studies used ERA-Interim reanalysis data (Di Giuseppe et al. 2016) and HRES forecasts (Di Giuseppe et al. 2020) for the fire weather danger indices. They also use different satellite data products: Di Giuseppe et al. (2016) used the burned area dataset from the GFED4 and Di Giuseppe et al. (2020) the FRP observations of MODIS.

In addition, Di Giuseppe et al. (2020) included agricultural, prescribed fires, and fires on shrublands or grasslands while we consider only forest fires. The number of years studied varies between 1 year and 11 years in previous studies, while we investigated 29 years (Di Giuseppe et al. 2016, Di Giuseppe et al. 2020). Interestingly, even though we also calculated the FWI based the yearly percentiles, their results (that are based on the yearly definition) do sometimes match better with the seasonal percentile definition (Table 4.1). Thus, the use of different datasets and different time periods between our and past studies are unlikely to lead to the exact same results. However, precisely because of these inherent discrepancies, the quite similar results are of even greater significance.

Lastly, when using reanalysis data for the FWI, it is important to remember that only the potential predictability can be determined and not the actual predictability (Di Giuseppe et al. 2016). Thus, the actual skill of the FWI predictions is only as good as the operational real-time forecasts as atmospheric forcings.

4.4.4 BIAS Score

A BIAS bigger than one for all pixels indicates that the FWI systematically overestimates the number of active fires (Figure 3.22). This means that there are a lot of false alarms as there are more estimated FDE than active fires (Figure 2.5). Since fires are rare events and the cost of a missed event is high in terms of human lives or valuable land, the overestimation (or overforecasting in the case of forecasts) may be justified (Di Giuseppe et al. 2020). In addition, the high fire danger can be correctly estimated but if there is no ignition it still counts as a false alarm. Hence, from the verification point of view, the identification of false alarms is not meaningful but rather a positively oriented metric that focuses on the hits and misses (Di Giuseppe et al. 2020). This confirms that the probability of detection f_{POD} is a good measure for the estimation of active fire occurrence.

5 Conclusion and Outlook

Wildfires are an essential part of our natural ecosystems but can have devastating impacts such as loss of resources and the deterioration of air quality. In recent decades, the total insured losses due to wildfires increased drastically. It is known that where fuel is available, weather is the most important factor shaping fire danger regimes. The meteorological conditions that would cause flames to spread if ignited are named fire weather, which is based on temperature, precipitation, relative humidity, and wind speed. Since fire weather danger is projected to increase in the future, it is of great importance to better understand the variability of fire danger.

Previous studies have shown that large-scale atmospheric circulation modulates the day-to-day surface weather and contributes to extremes like heatwaves and droughts. Therefore, large-scale weather atmospheric circulation could be also a potential dynamical driver for increased fire danger in Europe. In this study, we investigate the influence of persistent large-scale atmospheric circulation patterns, such as atmospheric blocking, on the spatiotemporal variability of fire weather danger and active fires across Europe. We use ERA-5 reanalysis data from ECMWF in the period of 1979-2020 and satellite-observed active fires retrieved from the AVHRR for the WMO period 1991-2019. Atmospheric blocks are identified and tracked as daily Z500 anomalies based on ERA5. To describe daily fire weather danger, we use the FWI and the FFMC based on the Canadian Fire Weather Index System provided by ERA5.

The extremely hot summer 2018 led to devastating and unprecedented fires in Scandinavia and to the most extreme heatwave on the Iberian Peninsula since 2003, which is why we use 2018 as a case study. The case study of the summer 2018 indicates a simultaneous variation of fire weather danger and active fires together with Z500. Several fire weather indices show a drastic increase in months when a block was present over Northern Europe. Therefore, the fire weather danger in Europe exhibits a strong spatiotemporal variability, which is confirmed by the climatologies of the FWI and FFMC. Generally, the mean FWI and day-to-day variability resemble the climatology of temperature, while the FFMC behaves similar to the variability of precipitation.

According to the case study of 2018, atmospheric blocking seems to modulate the fire weather danger and active fire occurrence. Therefore, we quantify the relevance of atmospheric blocking for co-located increased fire danger and occurrence. Our results show that over Northern and Western Europe more than 80% of all FWI EFDE and up to 100% of all FFMC EFDE occur simultaneously with a block at the same location, with a statistically significant relationship. This is a substantial portion of EFDE that occur co-located with atmospheric blocking. In Southern Europe, EFDE are not associated with blocking but rather with subtropical ridges northeast of the target region. Atmospheric blocking literally blocks the prevailing westerly large-scale atmospheric flow, leading to a positive pressure anomaly at the center

of the block and redirecting low pressure systems around the persistent blocking anticyclone. These long-lasting blocks lead to enhanced fire danger conditions in Northern and Western Europe and below average fire danger in Southern Europe. In accordance with previous studies, our study shows that high-latitude atmospheric blocking has a different impact on the occurrence of EFDE in Europe than subtropical ridges. Thus, for Northern Europe atmospheric blocking associated subsidence, a positive anomaly of solar radiation and the coupling with soil-moisture are suggested to be the dominant driver of EFDE. In Southern Europe, we have subtropical ridges located on the northeastern edge of the region and the most important mechanism contributing to EFDE might be diabatic warming by surface sensible heat fluxes.

Fire weather indices indicate only a potential fire danger and not whether there is actually a fire, which is dependent on an ignition. For this reason, we evaluate the capability of the FWI component to correctly estimate the occurrence of active fires. The so-called probability of detection (POD) evaluates the potential predictability of the FWI component by measuring its performance to effectively flag active fires. Despite several limitations of the AVHRR sensor such as the viewing geometries, the low saturation temperature of the MIR channel and detection problems due to clouds, the satellite data constitutes a continuous 29-year active fire dataset with a high resolution and is thus useful for a long-term climatological analysis as we perform.

The results of our POD analysis show that the FWI fire danger above the 90th percentile (>P90) can detect observed active fires in 38%-52% of the cases. The season in which active fires are detected best is winter and worst in summer. Regionally, the highest probability to detect active fires exhibits Eastern Mediterranean for >P90, while it is lowest in Western Mediterranean. However, including lower ranges (>P50 and >P70), Northern Europe performs much better than Southern Europe. Hence, we can say that in Eastern Mediterranean the FWI is able to detect active fires best for EFDE and in Northern Europe the performance is better for general above average fire danger conditions. This information on the capability of the FWI component in various regions and seasons is of great importance for fire management purposes in Europe and could be used to advance fire weather prediction in different regions and seasons.

If we look into the future, the projected changes in blocking occurrence are small but is still uncertain as climate models do not agree on the regional sign of changes. Competing effects in the Arctic and the Tropics could influence the future of blocks. On the one hand, the Artic Amplification reduces baroclinicity over midlatitudes, which leads to a weaker and wavier jet and subsequently to more blocks. On the other hand, upper-tropospheric warming in the tropics increases the baroclinicity that leads to a stronger and more zonal jet and thus less blocks. The exact governance mechanisms of future changes in blocking behavior are a current subject of research. For Europe, a small decrease in blocking

frequency is projected in summer for the end of the century and a shift of the blocks to the east and north. However, despite the uncertainty on the future of atmospheric blocking, fire weather danger is projected to become more extreme. It is therefore crucial to carry on with the research about fire weather danger, the fire occurrence and the large-scale atmospheric circulation as their driver and potential predictor.

In this last section, we present some potential further research topics that could be investigated. We include possible analyses that could not be done due to time reasons and other ideas that go beyond the scope of this thesis. This list is far from complete but should rather act as a starting point for novel research ideas:

- The presented analyses in this thesis could also be extended to other regions of the world that are affected regularly by wildfires such as North America or Australia.

- The fire weather danger during different European weather regimes could be investigated. For example, the results presented in this thesis indicate that Scandinavian blocking is of great relevance for co-located EFDE.

- In a further analysis, forecast data instead of reanalysis data could be used to assess the actual skill of the FWI predictions using operational real-time forecasts and if possible for a period of several years to ensure robust results.

- Instead of incorporating the lagged blocking influence of the past week, the influence of the blocking frequencies of the previous months on the present-day fire weather could be investigated.

- Another possible analysis would be to quantify the relevance of weather conditions and soil-moisture feedbacks. The desiccation of the soil and the subsequent increased evaporation could be a potential feedback mechanism influencing the fire weather danger. As we have seen, in summer 2018 there were two blocks present over Scandinavia in May and July. It would be interesting to investigate the relevance of the block in May (trough soil moisture feedbacks etc.) on the extreme fire danger in July compared to the influence of the block in July.

- Past studies showed that for heatwaves the origins of air parcels and its initial temperature are of minor importance but rather the processes of vertical motion and diabatic heating along the pathway. Thus, subsequent work should implement a Lagrangian analysis along the pathway of air parcels leading to EFDE to understand the underlying mechanisms that lead to EFDE.

- The thriving field of machine learning could also a potential tool to advance fire weather danger estimation and forecast. Lagerquist et al. (2017) developed a machine-learning model that uses self-organizing maps to predict extreme fire weather from synoptic patterns in Canada, which could also be applied to Europe.

- To optimize the prediction of the fire occurrence in the future, future investigations should focus on the definition of regional and seasonal thresholds for extreme fire danger. In that way, regional fire weather forecasts can be optimized according to the local vegetation and fire regime behavior.

6 Appendix

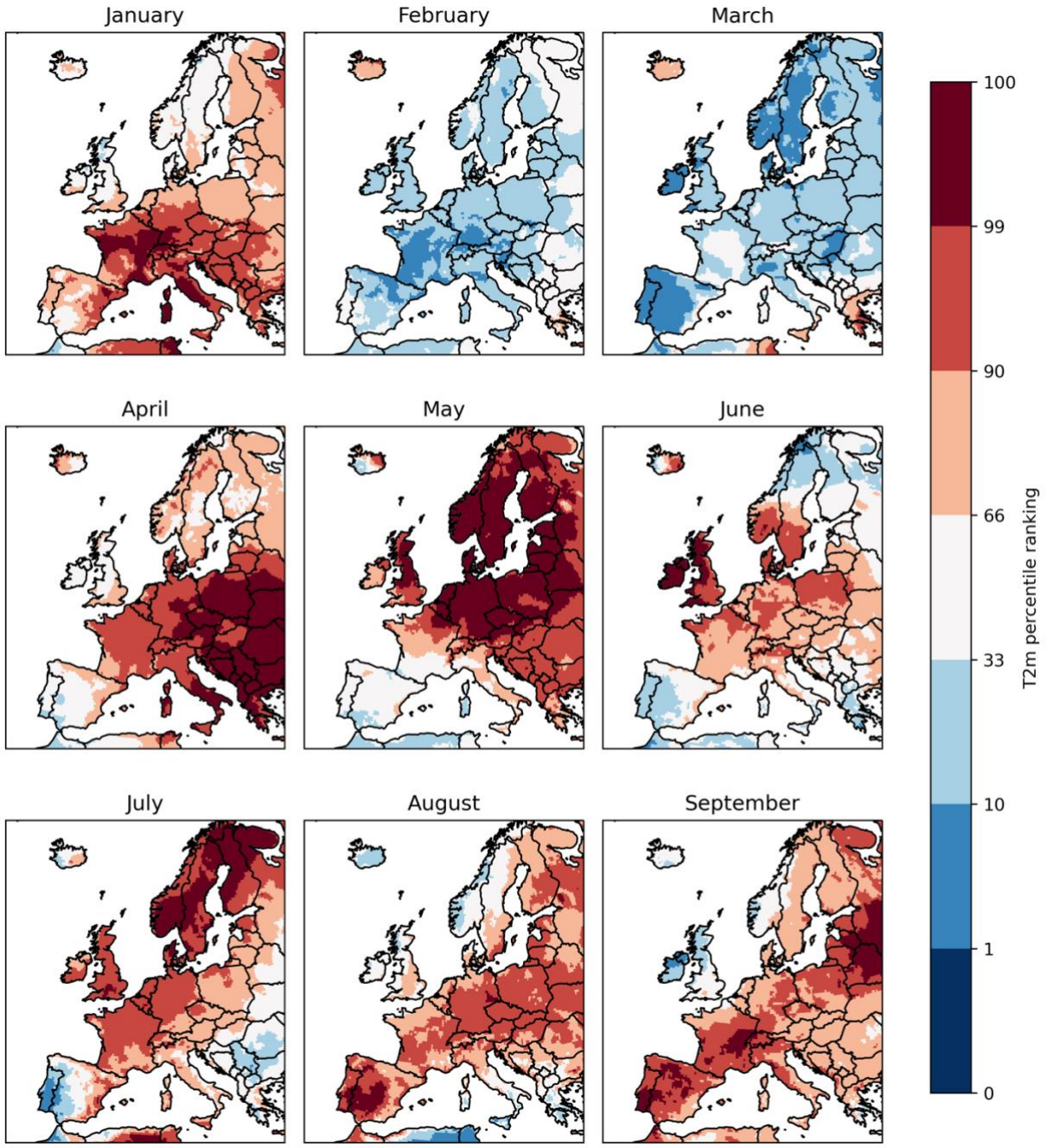

Figure 6.1: Monthly 2m temperature (percentile ranking, shading) for the year 2018. In addition to the monthly blocking frequency plot for the case study 2018 in Figure 3.4.

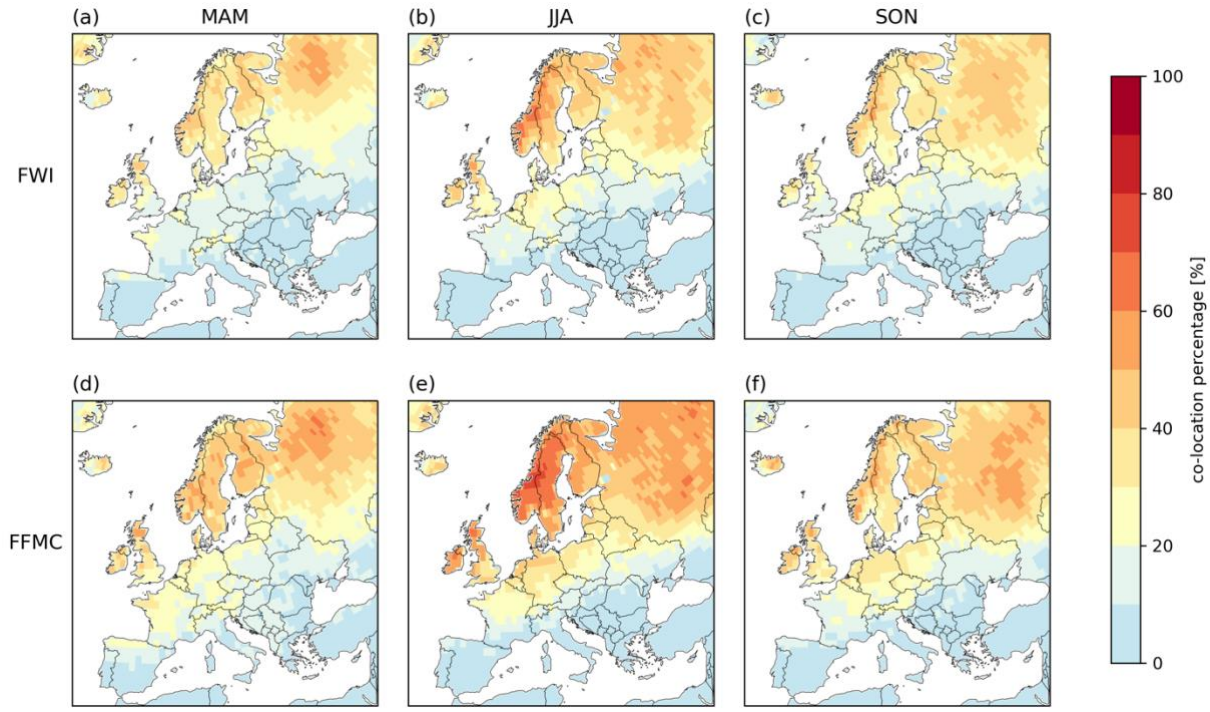

Figure 6.2: Percentage f_{EFDE} of extreme (P95) fire weather danger events (EFDE) occurring simultaneously with a blocking event at the same location for (a, d) spring, (b, e) summer and (c, f) autumn and for (a-c) the FWI and (d-f) the FFMC during 1979-2020. Without significance test, as P99 showed that only in Southern Europe non-significant.

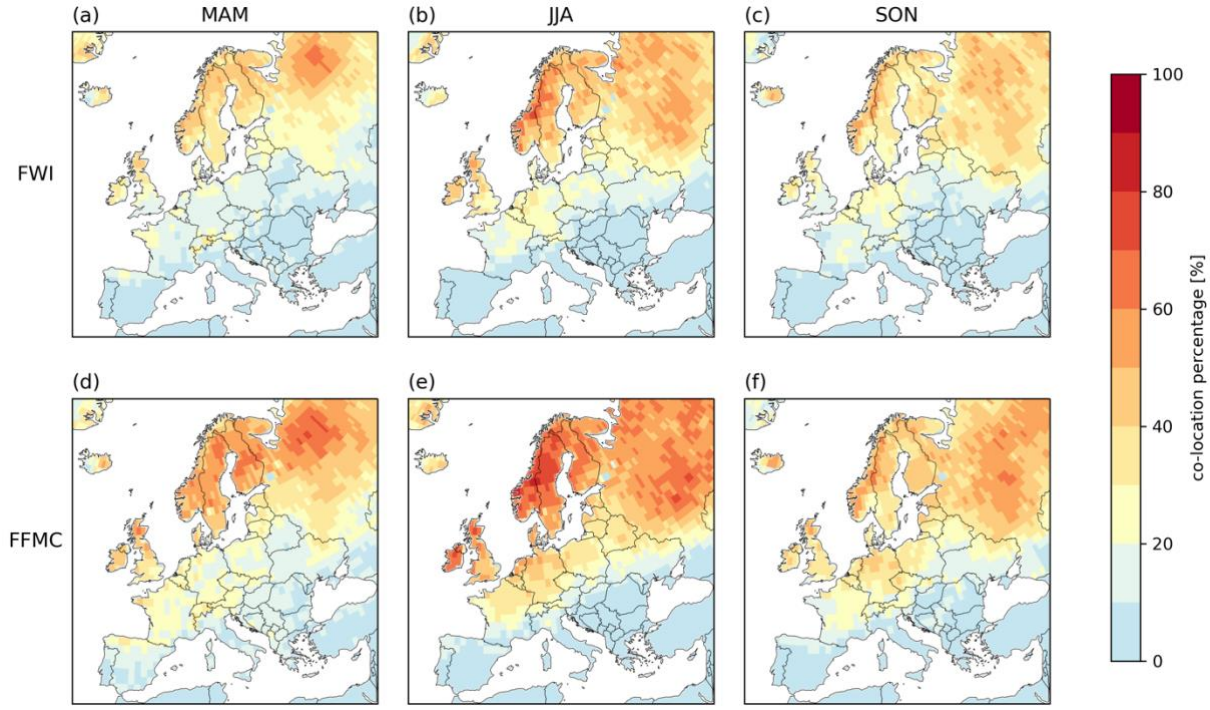

Figure 6.3: Percentage f_{EFDE} of extreme (P97) fire weather danger events (EFDE) occurring simultaneously with a blocking event at the same location for (a, d) spring, (b, e) summer and (c, f) autumn and for (a-c) the FWI and (d-f) the FFMC during 1979-2020. Without significance test, as P99 showed that only in Southern Europe non-significant.

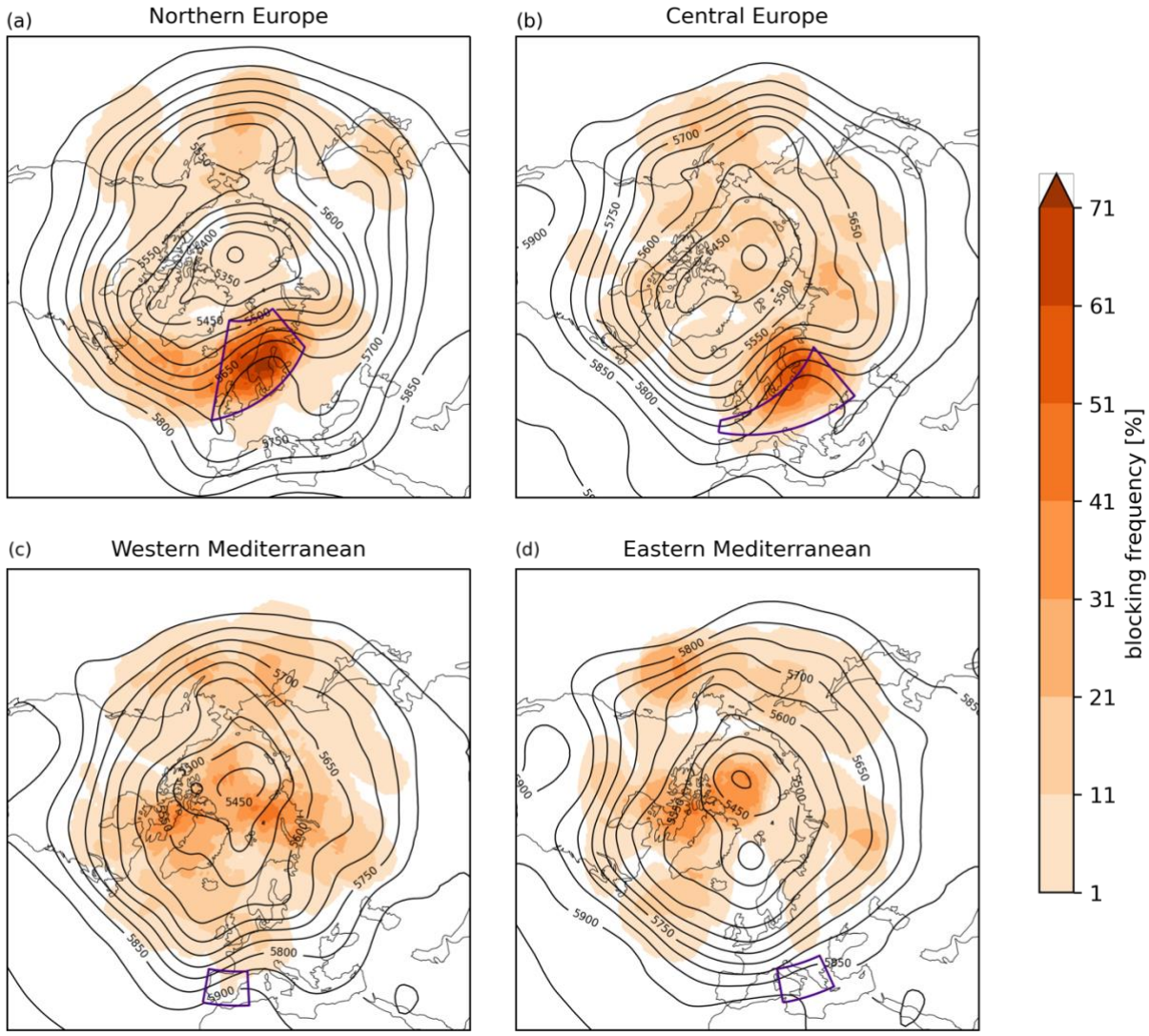

Figure 6.4: Composites of the relative blocking frequency (shaded, in %) and Z500 mean (black contours, in m) during area-weighted mean EFDE of the FWI in summer. The black boxes encompass each study region.

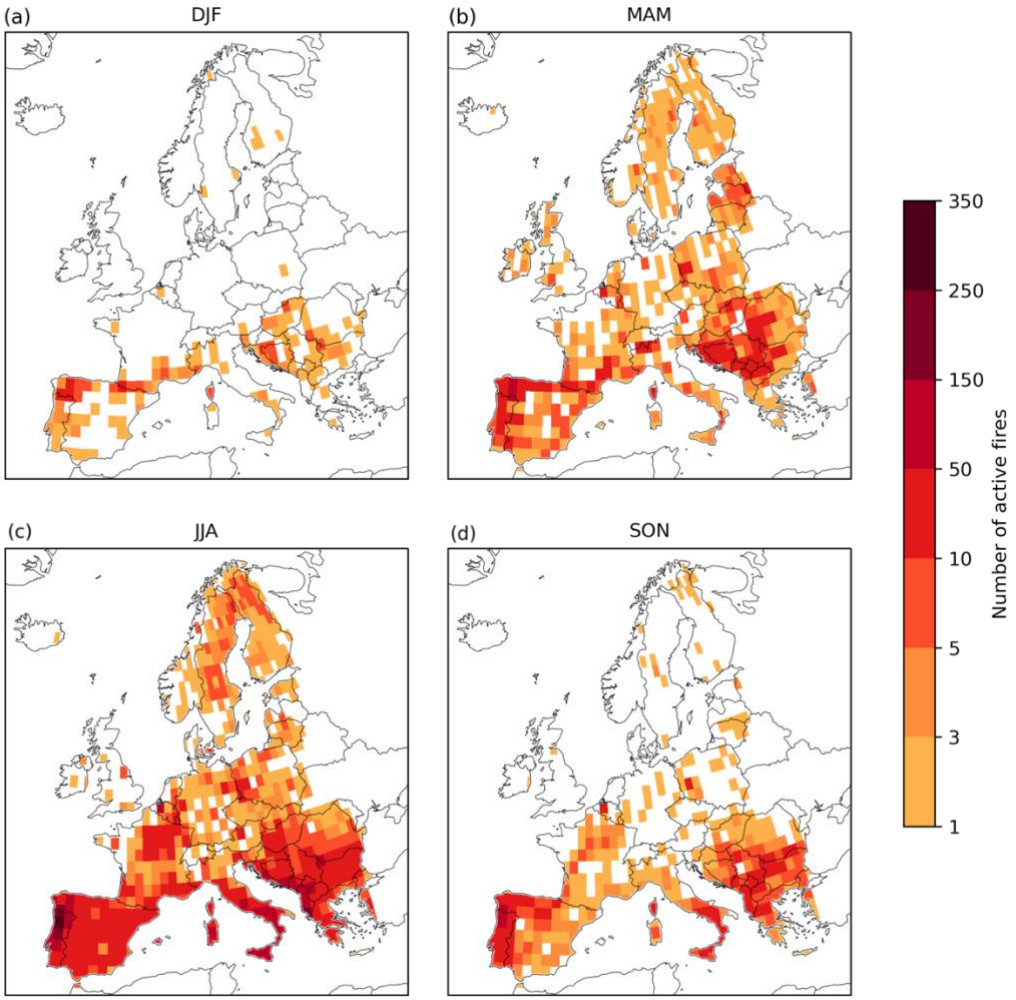

Figure 6.5: Seasonal observed number of active fires per grid cell in the period of 1991-2019 in Europe derived from AVHRR satellite data.

*Table 6.1: Regional area-weighted mean f_{POD} for the FWI above the P50 and P70 of its climatological values based on the seasonal distribution and for the four study regions. The numbers are derived from Figure 3.20 and the ones in **bold** are mentioned in the text.*

Region	> P50	> P70
Mediterranean West	74%	57%
Mediterranean East	86%	73%
Central Europe	90%	75%
Northern Europe	**92%**	**78%**

*Table 6.2: Seasonal area-weighted mean f_{POD} for the FWI above the P50 and P70 of its climatological values based on the seasonal distribution and for the four study regions. The numbers are derived from Figure 3.21 and the ones in **bold** are mentioned in the text.*

Season	> P50	> P70
MAM	89%	70%
JJA	**82%**	**66%**
SON	93%	81%
DJF	97%	89%

7 Bibliography

Abatzoglou, J. T., A. P. Williams, L. Boschetti, M. Zubkova and C. A. Kolden (2018) Global patterns of interannual climate–fire relationships, Global Change Biology, 24 (11) 5164–5175.

Barriopedro, D., P. M. Sousa, R. M. Trigo, R. García-Herrera and A. M. Ramos (2020) The Exceptional Iberian Heatwave of Summer 2018, Bulletin of the American Meteorological Society, 101 (1) 29 – 34.

Bedia, J., N. Golding, A. Casanueva, M. Iturbide, C. Buontempo and J. M. Gutiérrez (2018) Seasonal predictions of Fire Weather Index: Paving the way for their operational applicability in Mediterranean Europe, Climate Services, 9, 101–110, ISSN 2405-8807.

Bieli, M., S. Pfahl and H. Wernli (2015) A lagrangian investigation of hot and cold temperature extremes in europe, Quarterly Journal of the Royal Meteorological Society, 141.

Bonk, A. (2019) Fire occurrence and the current state of palaeofire reconstructions based on sedimentary charcoal from natural archives in Poland, Bulletin of Geography. Physical Geography Series, (17) 49–60.

Brunner, L., N. Schaller, J. Anstey, J. Sillmann and A. K. Steiner (2018) Dependence of Present and Future European Temperature Extremes on the Location of Atmospheric Blocking, Geophysical Research Letters, 45 (12) 6311–6320.

de Rigo, D., Libertà, G., Houston Durrant, T., Artés Vivancos, T., San-Miguel-Ayanz, J. (2017) Forest fire danger extremes in Europe under climate change: variability and uncertainty, EUR 28926 EN, Publications Office of the European Union, Luxembourg.

Di Giuseppe, F. (2021) User Guide - Fire danger indices historical data from the Copernicus Emergency Management Service.

Di Giuseppe, F., F. Pappenberger, F. Wetterhall, B. Krzeminski, A. Camia, G. Libertá and J. S. Miguel (2016) The Potential Predictability of Fire Danger Provided by Numerical Weather Prediction, Journal of Applied Meteorology and Climatology, 55 (11) 2469–2491.

Di Giuseppe, F., C. Vitolo, B. Krzeminski, C. Barnard, P. Maciel and J. San-Miguel (2020) Fire Weather Index: the skill provided by the European Centre for Medium-Range Weather Forecasts ensemble prediction system, Natural Hazards and Earth System Sciences, 20 (8) 2365–2378.

ECMWF (2020) Fact Sheet. <https://www.ecmwf.int/en/about/media-centre/focus/2020/fact-sheet-reanalysis>.

EEA (2009) Modelled three-monthly fire danger levels in Europe for 1961-1990 and 2071-2100 and change between these periods. <https://www.eea.europa.eu/data-and-maps/figures/modelled-three-monthly-fire-danger-levels-in-europe-for-1961-1990-and-2071-2100-and-change-between-these-periods>. European Environment Agency.

EEA (2021) Forest fires in Europe. <https://www.eea.europa.eu/ims/forest-fires-in-europe>. European Environment Agency.

EFFIS (n.d.) Fire Danger Forecast. <https://effis.jrc.ec.europa.eu/about-effis/technical-background/fire-danger-forecast>.

Flannigan, M. D. and B. M. Wotton (2001) Chapter 10 - Climate, Weather, and Area Burned, in E. A. Johnson and K. Miyanishi (eds.) Forest Fires, 351–373, Academic Press, San Diego, ISBN 978-0-12-386660-8.

Galizia, L. F., T. Curt, R. Barbero and M. Rodrigues (2022) Understanding fire regimes in Europe, International Journal of Wildland Fire, 31 (1) 56–66.

Ganteaume, A., A. Camia, M. Jappiot, J. San-Miguel-Ayanz, M. Long-Fournel and C. Lampin (2013) A Review of the Main Driving Factors of Forest Fire Ignition Over Europe, Environmental Management, 51 (3) 651–662, ISSN 1432-1009.

Giglio, L., J. D. Kendall and C. O. Justice (1999) Evaluation of global fire detection algorithms using simulated AVHRR infrared data, International Journal of Remote Sensing, 20 (10) 1947–1985.

Grams, C. M., R. Beerli, S. Pfenninger, I. Staffell and H. Wernli (2017) Balancing Europe's wind-power output through spatial deployment informed by weather regimes, Nature Climate Change, 7 (8) 557–562, ISSN 1758-6798.

Hersbach, H., B. Bell, P. Berrisford, S. Hirahara, A. Horányi, J. Muñoz-Sabater, J. Nicolas, C. Peubey, R. Radu, D. Schepers, A. Simmons, C. Soci, S. Abdalla, X. Abellan, G. Balsamo, P. Bechtold, G. Biavati, J. Bidlot, M. Bonavita, G. De Chiara, P. Dahlgren, D. Dee, M. Diamantakis, R. Dragani, J. Flemming, R. Forbes, M. Fuentes, A. Geer, L. Haimberger, S. Healy, R. J. Hogan, E. Hólm, M.

Janisková, S. Keeley, P. Laloyaux, P. Lopez, C. Lupu, G. Radnoti, P. de Rosnay, I. Rozum, F. Vamborg, S. Villaume and J.-N. Thépaut (2020) The ERA5 global reanalysis, Quarterly Journal of the Royal Meteorological Society, 146 (730) 1999–2049, jul 2020, ISSN 0035-9009.

Hoinka, K. P., A. Carvalho and A. I. Miranda (2009) Regional-scale weather patterns and wildland fires in central Portugal, International Journal of Wildland Fire, 18, 36–49.

Horton, R. M., J. S. Mankin, C. Lesk, E. Coffel and C. Raymond (2016) A Review of Recent Advances in Research on Extreme Heat Events, Current Climate Change Reports, 2 (4) 242–259, ISSN 2198-6061.

Hostetler, S. W., P. J. Bartlein and J. R. Alder (2018) Atmospheric and Surface Climate Associated With 1986–2013 Wildfires in North America, Journal of Geophysical Research: Biogeosciences, 123 (5) 1588–1609.

IPCC (2021) Climate Change 2021: The Physical Science Basis. Contribution of Working Group I to the Sixth Assessment Report of the Intergovernmental Panel on Climate Change.

Iturbide, M., J. M. Gutiérrez, L. M. Alves, J. Bedia, R. Cerezo-Mota, E. Cimadevilla, A. S. Cofiño, A. Di Luca, S. H. Faria, I. V. Gorodetskaya, M. Hauser, S. Herrera, K. Hennessy, H. T. Hewitt, R. G. Jones, S. Krakovska, R. Manzanas, D. Mart´-Castro, G. T. Narisma, I. S. Nurhati, I. Pinto, S. I. Seneviratne, B. van den Hurk and C. S. Vera (2020) An update of IPCC climate reference regions for subcontinental analysis of climate model data: definition and aggregated datasets, Earth System Science Data, 12 (4) 2959–2970.

Jain, P. and M. Flannigan (2021) The Relationship between the Polar Jet Stream and Extreme Wildfire Events in North America, Journal of Climate, 34 (15) 6247–6265.

Jolly, W. M., M. A. Cochrane, P. H. Freeborn, Z. A. Holden, T. J. Brown, G. J. Williamson and D. M. J. S. Bowman (2015) Climate-induced variations in global wildfire danger from 1979 to 2013, Nature Communications, 6 (1) 7537, ISSN 2041-1723.

Kalluri, S., C. Cao, A. Heidinger, A. Ignatov, J. Key and T. Smith (2021) The Advanced Very High Resolution Radiometer: Contributing to Earth Observations for over 40 Years, Bulletin of the American Meteorological Society, 102 (2) E351 – E366.

Kautz, L.-A., O. Martius, S. Pfahl, J. G. Pinto, A. M. Ramos, P. M. Sousa and T. Woollings (2022) Atmospheric blocking and weather extremes over the Euro-Atlantic sector – a review, Weather and Climate Dynamics, 3 (1) 305–336.

Koenker, R. (2005) Quantile Regression, Econometric Society Monographs, Cambridge University Press.

Lagerquist, R., M. D. Flannigan, X. Wang and G. A. Marshall (2017) Automated prediction of extreme fire weather from synoptic patterns in northern Alberta, Canada, Canadian Journal of Forest Research, 47 (9) 1175–1183.

Lenggenhager, S. and O. Martius (2019) Atmospheric blocks modulate the odds of heavy precipitation events in Europe, Climate Dynamics, 53 (7) 4155–4171, ISSN 1432-0894.

Macias Fauria, M. and E. A. Johnson (2006) Large-scale climatic patterns control large lightning fire occurrence in Canada and Alaska forest regions, Journal of Geophysical Research: Biogeosciences, 111 (G4).

Mastrantonas, N., P. Herrera-Lormendez, L. Magnusson, F. Pappenberger and J. Matschullat (2021) Extreme precipitation events in the Mediterranean: Spatiotemporal characteristics and connection to large-scale atmospheric flow patterns, International Journal of Climatology, 41 (4) 2710–2728.

Matsueda, M. and H. Endo (2017) The robustness of future changes in Northern Hemisphere blocking: A large ensemble projection with multiple sea surface temperature patterns, Geophysical Research Letters, 44 (10) 5158–5166.

Miralles, D. G., P. Gentine, S. I. Seneviratne and A. J. Teuling (2019) Land–atmospheric feedbacks during droughts and heatwaves: state of the science and current challenges, Annals of the New York Academy of Sciences, 1436 (1) 19–35.

Miralles, D. G., A. J. Teuling, C. C. van Heerwaarden and J. Vilà-Guerau de Arellano (2014) Mega-heatwave temperatures due to combined soil desiccation and atmospheric heat accumulation, Nature Geoscience, 7 (5) 345–349, ISSN 1752-0908.

Peña-Angulo, D., F. Reig-Gracia, F. Domínguez-Castro, J. Revuelto, E. Aguilar, G. van der Schrier and S. M. Vicente-Serrano (2020) ECTACI: European Climatology and Trend Atlas of Climate Indices (1979–2017), Journal of Geophysical Research: Atmospheres, 125 (16) 1–17.

Pfahl, S. (2014) Characterising the relationship between weather extremes in Europe and synoptic circulation features, Natural Hazards and Earth System Sciences, 14 (6) 1461–1475.

Pfahl, S. and H. Wernli (2012a) Quantifying the relevance of atmospheric blocking for co-located temperature extremes in the northern hemisphere on (sub-)daily time scales, Geophysical Research Letters, 39 (12).

Pfahl, S. and H. Wernli (2012b) Quantifying the Relevance of Cyclones for Precipitation Extremes, Journal of Climate, 25 (19) 6770–6780.

Rasilla, D. F., J. C. García-Codron, V. Carracedo and C. Diego (2010) Circulation patterns, wildfire risk and wildfire occurrence at continental Spain, Physics and Chemistry of the Earth, Parts A/B/C, 35 (9) 553–560, ISSN 1474-7065.

Ruffault, J., V. Moron, R. M. Trigo and T. Curt (2017) Daily synoptic conditions associated with large fire occurrence in Mediterranean France: evidence for a wind-driven fire regime, International Journal of Climatology, 37 (1) 524–533.

Santos, J. A., S. Pfahl, J. G. Pinto and H. Wernli (2015) Mechanisms underlying temperature extremes in Iberia: a Lagrangian perspective, Tellus A: Dynamic Meteorology and Oceanography, 67 (1) 26032.

Schwierz, C., M. Croci-Maspoli and H. C. Davies (2004) Perspicacious indicators of atmospheric blocking, Geophysical Research Letters, 31 (6).

Sillmann, J. and M. Croci-Maspoli (2009) Present and future atmospheric blocking and its impact on European mean and extreme climate, Geophysical Research Letters, 36 (10).

Sousa, P. M., R. M. Trigo, D. Barriopedro, P. M. M. Soares and J. A. Santos (2018) European temperature responses to blocking and ridge regional patterns, Climate Dynamics, 50 (1) 457–477, ISSN 1432-0894.

Spensberger, C., E. Madonna, M. Boettcher, C. M. Grams, L. Papritz, J. F. Quinting, M. Röthlisberger, M. Sprenger and P. Zschenderlein (2020) Dynamics of concurrent and sequential Central European and Scandinavian heatwaves, Quarterly Journal of the Royal Meteorological Society, 146 (732) 2998–3013.

Stéfanon, M., F. D'Andrea and P. Drobinski (2012) Heatwave classification over europe and the mediterranean region, Environmental Research Letters, 7, 014023, 03 2012.

SwissRe (2021) Yet more wildfires. <https://www.swissre.com/risk-knowledge/mitigating-climate-risk/yet-more-wildfires.html>.

Teng, H. and G. Branstator (2017) Causes of Extreme Ridges That Induce California Droughts, Journal of Climate, 30 (4) 1477–1492.

UNEP (2022) Spreading like Wildfire – The Rising Threat of Extraordinary Landscape Fires. A United Nations Environment Programme (UNEP) Rapid Response Assessment. Nairobi.

Van Wagner, C. E. (1987) Development and structure of the Canadian Forest Fire Weather Index System, 1–35.

Viegas, D., G. Bovio, A. Ferreira, A. Nosenzo and B. Sol (1999) Comparative Study of Various Methods of Fire Danger Evaluation in Southern Europe, International Journal of Wildland Fire, 9, 235–246.

Vitolo, C., F. Di Giuseppe, C. Barnard, R. Coughlan, J. San-Miguel-Ayanz, G. Libertá and B. Krzeminski (2020) ERA5-based global meteorological wildfire danger maps, Scientific Data, 7 (1) 216, ISSN 2052-4463.

Vitolo C, Di Giuseppe F, D'Andrea M (2018) Caliver: An R package for CALIbration and VERification of forest fire gridded model outputs. PLoS ONE 13(1): e0189419.

Wastl, C., C. Schunk, M. Lüpke, G. Cocca, M. Conedera, E. Valese and A. Menzel (2013) Large- scale weather types, forest fire danger, and wildfire occurrence in the Alps, Agricultural and Forest Meteorology, 168, 15–25, ISSN 0168-1923.

Weber, H. and S. Wunderle (2019) Drifting Effects of NOAA Satellites on Long-Term Active Fire Records of Europe, Remote Sensing, 11 (4), ISSN 2072-4292.

Weber 2021. In preparation.

Woollings, T., D. Barriopedro, J. Methven, S.-W. Son, O. Martius, B. Harvey, J. Sillmann, A. R. Lupo and S. Seneviratne (2018) Blocking and its Response to Climate Change, Current Climate Change Reports, 4 (3) 287–300, ISSN 2198-6061.

Yano, J.-I., M. Z. Ziemiański, M. Cullen, P. Termonia, J. Onvlee, L. Bengtsson, A. Carrassi, R. Davy, A. Deluca, S. L. Gray, V. Homar, M. Köhler, S. Krichak, S. Michaelides, V. T. J. Phillips, P. M. M. Soares and A. A. Wyszogrodzki (2018) Scientific Challenges of Convective-Scale Numerical Weather Prediction, Bulletin of the American Meteorological Society, 99 (4) 699–710.

Zschenderlein, P., A. H. Fink, S. Pfahl and H. Wernli (2019) Processes determining heat waves across different european climates, Quarterly Journal of the Royal Meteorological Society, 145 (724) 2973–2989.

8 Acknowledgements

A big thank you goes to my advisor Daniel Steinfeld from the University of Bern. I am very grateful for his support and his countless useful inputs for the thesis. He always took the time to discuss a lot of different topics and answer urgent questions. I would also like to thank my two supervisors Stefan Brönnimann and Olivia Romppainen-Martius from the University of Bern, for their support, valuable exchanges in our meetings, and the opportunity to write my thesis in their group. Many thanks are also owed to Helga Weber from the Remote Sensing Group at the University of Bern, for the many very interesting discussions and question answering about Satellite Data. Another thanks goes to my fellow students for helpful discussions and their technical and also mental support. Last but not least, I want to thank my family and friends for their support, patience and inputs during the last year.

Declaration of consent

on the basis of Article 30 of the RSL Phil.-nat. 18

Name/First Name: Herrmann Michael

Registration Number: 16-721-565

Study program: M.Sc. in Climate Sciences

Bachelor ☐ Master ☑ Dissertation ☐

Title of the thesis: Forest fire and its relationship to large-scale atmospheric circulation

Supervisor: Prof. Dr. Stefan Brönnimann and Prof. Dr. Olivia Romppainen-Martius

I declare herewith that this thesis is my own work and that I have not used any sources other than those stated. I have indicated the adoption of quotations as well as thoughts taken from other authors as such in the thesis. I am aware that the Senate pursuant to Article 36 paragraph 1 litera r of the University Act of 5 September, 1996 is authorized to revoke the title awarded on the basis of this thesis.

For the purposes of evaluation and verification of compliance with the declaration of originality and the regulations governing plagiarism, I hereby grant the University of Bern the right to process my personal data and to perform the acts of use this requires, in particular, to reproduce the written thesis and to store it permanently in a database, and to use said database, or to make said database available, to enable comparison with future theses submitted by others.

Bern, 27th of October 2022

Place/Date

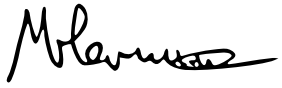

Signature